AFRL-RH-FS-TR-2014-0003

In Vivo Multimodal Imaging of NF-κB (p5) Spatial and Temporal Activation Following Light Injury in the Mouse Retina

Ginger M. Pocock
Brent J. Lavey
Human Effectiveness Directorate
Directed Energy Bioeffects Division
Optical Radiation Branch

Adam Boretsky
Praveena Gupta
Gracie Vargas
Wenbo Zhang
Massoud Motamedi
The University of Texas Medical Branch at Galveston,
Department of Biomedical Engineering

Heuy-Ching H Wang
United States Army of Institutes of Surgical Research

January 15, 2014

Interim Report for January 2010 to January 2012

DESTRUCTION NOTICE – Destroy by any method that will prevent disclosure of contents or reconstruction of this document.

Air Force Research Laboratory
711th Human Performance Wing
Human Effectiveness Directorate
Bioeffects Division
Optical Radiation Bioeffects
JBSA Fort Sam Houston, Texas 78234

NOTICE AND SIGNATURE PAGE

Using Government drawings, specifications, or other data included in this document for any purpose other than Government procurement does not in any way obligate the U.S. Government. The fact that the Government formulated or supplied the drawings, specifications, or other data does not license the holder or any other person or corporation; or convey any rights or permission to manufacture, use, or sell any patented invention that may relate to them.

Qualified requestors may obtain copies of this report from the Defense Technical Information Center (DTIC) (http://www.dtic.mil).

"In Vivo Multimodal Imaging of NF-κB (p5) Spatial and Temporal Activation Following Light Injury in the Mouse Retina"

(AFRL-RH-FS-TR - 2014 - 0003) has been reviewed and is approved for publication in accordance with assigned distribution statement.

ROCKWELL.BENJAMIN.A.1231305358

Digitally signed by ROCKWELL.BENJAMIN.A.1231305358
DN: c=US, o=U.S. Government, ou=DoD, ou=PKI, ou=USAF, cn=ROCKWELL.BENJAMIN.A.1231305358
Date: 2014.01.30 16:02:01 -06'00'

BENJAMIN A. ROCKWELL, DR-IV, DAF
Work Unit Manager
Optical Radiation Bioeffects Branch

WOLF.STEPHEN.P.1108359664

Digitally signed by WOLF.STEPHEN.P.1108359664
DN: c=US, o=U.S. Government, ou=DoD, ou=PKI, ou=USAF, cn=WOLF.STEPHEN.P.1108359664
Date: 2014.02.25 14:58:52 -06'00'

STEPHEN P. WOLF, LT COL, USAF, BSC
Acting Chief, Bioeffects Division
Human Effectiveness Directorate
711th Human Performance Wing
Air Force Research Laboratory

This report is published in the interest of scientific and technical information exchange, and its publication does not constitute the Government's approval or disapproval of its ideas or findings.

REPORT DOCUMENTATION PAGE

Form Approved
OMB No. 0704-0188

1. REPORT DATE *(DD-MM-YYYY)*	**2. REPORT TYPE**	**3. DATES COVERED *(From - To)***
15-01-14	Interim Technical Report	January 2010-January 2012

4. TITLE AND SUBTITLE
In vivo Multimodal Imaging of NF-κB (p5) Spatial and Temporal Activation Following Light Injury in the Mouse Retina

5a. CONTRACT NUMBER
FA8650-08-D-6930

5b. GRANT NUMBER

5c. PROGRAM ELEMENT NUMBER
0602202F

6. AUTHOR(S)
Ginger M. Pocock, Brent J. Lavey, Adam Boretsky, Praveena Gupta, Gracie Vargas, Wenbo Zhang, Heuy-Ching H Wang, and Massoud Motamedi

5d. PROJECT NUMBER
7757

5e. TASK NUMBER
HD

5f. WORK UNIT NUMBER
04

7. PERFORMING ORGANIZATION NAME(S) AND ADDRESS(ES)
Air Force Research Laboratory
711th Human Performance Wing
Human Effectiveness Directorate
Bioeffects Division
Optical Radiation Bioeffects
Fort Sam Houston, Texas 78234

8. PERFORMING ORGANIZATION REPORT NUMBER

9. SPONSORING / MONITORING AGENCY NAME(S) AND ADDRESS(ES)
Air Force Research Laboratory
711th Human Performance Wing
Human Effectiveness Directorate
Bioeffects Division
Optical Radiation Bioeffects
Fort Sam Houston, Texas 78234

10. SPONSOR/MONITOR'S ACRONYM(S)
711 HPW/RHDO

11. SPONSOR/MONITOR'S REPORT NUMBER(S)
AFRL-RH-FS-TR-2014-0003

12. DISTRIBUTION / AVAILABILITY STATEMENT
Distribution A: Approved for public release; distribution unlimited (approval given by local Public Affairs Office TSRL-PA-14-0038)

13. SUPPLEMENTARY NOTES

14. ABSTRACT
BALB/c and C57BL/6 wild type mice and (cis-NF-κB-EGFP) transgenic mouse model were used to perform *in vivo* experiments of laser-induced thermal damage to the retina. A Heidelberg Spectralis HRA confocal scanning laser ophthalmoscope with a spectral domain optical coherence tomographer was used to obtain fundus and cross-sectional images of laser induced injury in the retina. Sub-threshold, threshold, and supra-threshold lesions were imaged up to 10 days post exposure using optical coherence tomography (OCT), infrared reflectance, red-free reflectance, fluorescence angiography, and autofluorescence imaging modalities. The spatial and temporal activation of Nuclear factor-kappa B (NF-κB) (p65) was monitored in the retina of the cis-NF-κB-EGFP mouse. In addition, EGFP basal expression in brain and retinal tissue from the cis-NF-κB-EGFP was characterized using two-photon imaging. Injured and control eyes were enucleated at discrete time points following laser exposure for cryosectioning and confocal microscopy to determine localization of NF-κB dependent enhanced green fluorescent protein (EGFP) reporter gene expression within the retina. Furthermore, immunohistochemistry for GFAP, IBA-1, NeuN, CD65, and glutamine synthetase were used to examine the retinal structures and cell population expressing upregulated activation of p65 as a result of laser induced injury.

15. SUBJECT TERMS

16. SECURITY CLASSIFICATION OF: Unclassified			**17. LIMITATION OF ABSTRACT**	**18. NUMBER OF PAGES**	**19a. NAME OF RESPONSIBLE PERSON**
a. REPORT	**b. ABSTRACT**	**c. THIS PAGE**			LTC Michelle Aaron
U	U	U	U	42	**19b. TELEPHONE NUMBER *(include area code)*** NA

Standard Form 298 (Rev. 8-98)
Prescribed by ANSI Std. 239.18

This Page Intentionally Left Blank

TABLE OF CONTENTS

TABLE OF FIGURES

LIST OF TABLES

1 INTRODUCTION

Lasers in a clinical setting are used to treat and manage wet age-related macular degeneration (AMD), diabetic retinopathy, and other retinal disorders.[1] There is a strong desire to find strategies to limit injury to surrounding neural tissue after the delivery of laser energy to the retina. Glucocorticoids inhibit NF-κB driven activation of cytokines by means which are not completely understood but are commonly used.[2,3] Intravitreal steroidal injections have been used as thermal laser therapy, for treatment of accidental laser injury, and to mitigate retinal disease.[4–8] Anti-inflammatory treatments inhibit NF-κB driven activation of cytokines and chemokines, are commonly used to treat laser injuries, and have been shown to improve photoreceptor survival in the primate.[4, 9–12]

The degree and type of retinal damage is dependent upon the light exposure parameters.[13–16] The primary effect of thermal light damage is necrosis of the central area of laser energy deposition with a surrounding area of injured tissue.[16–18] The morphology of the injury zone is dependent upon the beam profile shape (e.g. Gaussian distribution) and energy distribution at the retina. The outer radial zone of the central injury may undergo apoptosis or recovery.[17,18] Damage to adjacent retinal layers, such as the photoreceptors and choriocapillaris, may occur from thermal conduction Furthermore, secondary effects of laser damage, such as the release of excitotoxic molecules, may contribute to the lesion appearance and size over the course of time.[19] Photochemical damage occurs from light-triggered chemical reactions, causing the formation of free radicals, which can cause protein modification and lipid peroxidation in the retina.[16] Photo-oxidative stress has been implicated in both thermal and photochemical damage to the retina.[13,14] Laser injury to the retina is well understood at the macroscopic level, but efforts still need to be made to understand the molecular signaling events associated with the regime of laser injury and or any therapeutic effects.

The molecular response of the mouse and rat retina to “light damage” has been well studied, as light induced damage is the most assessable model to study retinal degeneration.[20–24] NF-κB is a family of heterodimeric transcription factors that regulates stress responses in a variety of experimental stimuli by exerting a modulatory effect on apoptosis, cell survival, and inflammation.[25–27] Experimental conditions that activate NF-κB include reactive oxygen species (ROS), pathogens, injury shock waves, and ischemia all of which can be induced by laser injury.[28–35]

In addition, the gaining acceptance of retinal laser phototherapy beckons detailed understanding of the molecular mechanisms governing the accelerated tissue repair and if any negative consequences of treatment exist.[36–43] The “nuts and bolts” of the low-level light hypothesis is that the accelerated healing from exposure to “low-energy light” exposure is the result of differences in the redox potential from a baseline state. The absorption of light by cytochrome c in the mitochondria increases the redox potential in the direction of greater oxidation. The increased oxidation “switches” the cell into a defense state possibly by way of transcription factors and pathways related to oxidative metabolism which initiates the increase production of antioxidants. Potential transcription factors that may initiate the “switch” include NF-κB.[40, 44–46]

Using knock-in/out mice, researchers investigating molecular signaling pathways and their effect on the cellular response to neural disease and injury have been afforded the ability to monitor

these pathways over several time points without the need for histology. Previous research has established transgenic mice as a reliable model for studying injury from light exposure to the retina, cornea, and skin.[22,47,48] Studies examining NF-κB activation or inactivation expression patterns within the retina have had to rely solely on traditional methods such immunohistochemistry, western blot, real-time RT-PCR, and histology which are limited to a single time point for anatomical information or expression levels. In this study we examine the spatial and temporal NF-κB activation in promoting inflammation following thermal light damage *in vivo* using the cis-NF-κB-EGFP reporter mouse in addition to using fluorescence microscopy. Validation of the cis-NF-κB-EGFP mouse model for light induced damage studies may allow *in vivo* investigations regarding therapeutic strategies centered on NF-κB activation for treatment protocol development and possible insights into unwanted secondary effects as a result of treatment. In particular, molecular imaging after photochemical and thermal light damage may provide insight into the differences in the light damage process. In addition, results may provide an insight into the localization of the NF-κB transcription signature related to inflammation, immunity, nerve injury induced apoptosis, and neurodegeneration.

2 MATERIALS AND METHODS

2.1 Animal Preparation

All transgenic mice used had been backcrossed greater than 7 times to a C57BL/6 background. Age matched (6-15 weeks) control wildtype mice were also the C57BL/6 strain. A cis-NF-κB-EGFP breeding trio was provided by Christian Jobin (University of North Carolina at Chapel Hill). The cis-NF-κB-EGFP mice were created using a gene-targeting approach to integrate a single copy of the NF-κB reporter construct into a single locus of the HPRT gene.[49] A total of 26 male cis-NF-κB-EGFP (6-8 months old) and 3 retired breeders were used to monitor changes associated with laser exposure from 4 hours up to 7 days later. One subject was followed up 25 days later. Experiments were performed according to regulations of the Association for Research in Vision and Ophthalmology (ARVO) Statement for the Use of Animals in Ophthalmic and Vision Research. The animals involved in this study were procured, maintained, and used in accordance with the Federal Animal Welfare Act, "Guide for the Care and Use of Laboratory Animals," prepared by the Institute of Laboratory Animal Resources National Research Council, and Army Regulation 40-33, SECNAVISNT 3900.38C, AFMAN 40-401(I), DARPAINST 18, USUHSINST 3203, "The Care and Use of Laboratory animals in DOD Programs." All experimental methods were approved by the Institutional Animal Care and Use Committees of the University of Texas Medical Branch in Galveston, TX and Tri-Services Research Laboratory Fort Sam Houston, TX.

2.2 Laser Induced Retinal Injury

Prior to retinal lesion placement and imaging, mice were anesthetized with isoflurane (1% - 2%). Once restrained, topical ocular anesthetic (Proparacaine HCl) eye drops were administered and eyelids were retracted using sterilized retractors. Corneal hydration was maintained throughout imaging by applying 0.5% methylcellulose lubricating eye drops (Alcon Laboratories, Ft. Worth, TX) every 2-3 minutes. An adjustable, heated platform was used to maintain body temperature and allow appropriate positioning of the eye for imaging and photocoagulation. A 3.2 mm fundus laser lens (Ocular Instruments) was used to visualize the fundus for lesion placement in the reti-

na. A Coherent Ultima 2000 argon laser operating at 514 nm in conjunction with a Zeiss Model 30 SL-M slit lamp was used to create up to 10 lesion sites surrounding the optic nerve head in one eye per mouse. Lesions were characterized as sub-threshold, threshold, or supra-threshold based on lesion appearance in red free (RF) fundus images. All reported laser energies were measured at the cornea, and exposures were made in one eye (OD) with the other eye serving as a control (OS). Power levels of 8.4 mW, 14.6 mW, and 28 mW were used to induce retinal injury at the sub-threshold, threshold, and supra-threshold level, respectively. Exposure time was set at 0.1 s for all exposures and a laser spot size of 100 μm and 500 μm at the cornea was selected.

A subset of retired breeders and 6-8 week old cis-NF-κB-EGFP mice (n=6) and wildtype mice (n=3) were used to establish lesion dosimetry and imaging protocol for capturing EGFP fluorescence generated as a result of injury. The remaining 17 mice were divided into 4 exposure categories (Table 1). Group 1 (n=3) received sub-threshold exposures at a laser exposure of 8.4 mW at the cornea. Group 2 (n=5) was exposed to 14.6 mW resulting in threshold injury. Supra-threshold exposures from 28.9 mW laser exposures were administered to Group 3 (n=6).

Table 1: Laser exposure parameters for all mice

Power (mW)	Num. of Exposures	Radiant Exposure (J/cm^2)	Injury Grade
8.4	15 (n=3)	10.6	Sub-threshold
14.6	30 (n=5)	18.6	Threshold
28.9	49 (n=6)	36.8	Supra-threshold
28.9	4 (n=3)	14.7	Supra-threshold

2.3 *In Vivo* Imaging

2.3.1 Scanning Laser Ophthalmoscope.

The Spectralis Heidelberg retinal angiograph + spectral domain optical coherence tomography (HRA+OCT) (Spectralis; Heidelberg Engineering, Heidelberg, Germany) which contains a confocal scanning laser ophthalmoscope (cSLO) with an OCT, was used to obtain EGFP fluorescence signal emanating from the retina in addition to fundus and retinal cross sections. A 25 diopter lens was mounted on the front imaging end of the Spectralis to image mice. A small blanket was placed underneath the mouse to dampen breathing artifacts in retinal images. The cSLO features one argon wavelength (488 nm) and two infrared diode lasers (790/820 nm) which were used to obtain images of the fundus using infrared (IR) reflectance, RF reflectance, fluorescein angiography (FA), and autofluorescence (AF). All fundus images were acquired in the high resolution mode (1536 x 1536 pixels) over a 30° x 30° or 20° x 20° (1024 x 1024 pixels) field of view (FOV). The cSLO scan rate is 15 frames/sec and multiple frames (greater than 12) were averaged to reduce image noise. To compensate for eye movement, an eye tracker was used to create images in which the movement artifact was removed or minimized. EGFP fluorescence was excited using with a wavelength of 488 nm. Fluorescence emission was detected between 500 and 700 nm. In addition, reflectance and fluorescence images were collected simultaneously

with varying focus settings to allow sectional scans through the mouse retina to investigate the depth location of the detected fluorescence signal. A subset of uninjured transgenic mice (n=5) were imaged to examine any possible effects caused by the imaging laser.

2.3.2 Optical Coherence Tomography

SD-OCT (λ=870 nm) volume scans and line scans were acquired for a subset of wildtype and transgenic mice to characterize changes in lesion morphology over time in association with upregulated NF-κB expression related to injury. Each B-scan consists of 1536 or 768 A-scans acquired at a scan rate of 40,000 A-scans per second to generate OCT cross-sectional images. Raster scans for volumetric representations and measurements consisted of 49 B-scans spaced approximately 3.8 μm apart covering a 548 x 183 μm area. Subject's retinas were imaged immediately following laser exposure, 4 hours, 8 hours, 12 hours, 1-14 days, and up to 5 months after injury. Eye tracking based on blood vessel patterns was used to collect images of lesions for time course follow up.

To set the transverse scale of OCT B-scans, 12 μm polystyrene beads were injected into the vitreous of one subject. The lateral resolution was calibrated via the corneal curvature setting in the Eye Explorer software (Heidelberg Engineering) to correctly measure bead size. Spectralis OCT raw data files were imported into Matlab 2009b (MathWorks Inc., Natick, MA) to generate 32-bit two dimensional grayscale images of SD-OCT B-scans. The image stack was then imported into the Avizo 6.3 (Visualization Sciences Group, Burlington, MA) software to create 3D volumetric renderings of the retina from the raster scan data sets.

2.4 Fluorescence Microscopy of Cryosections and Retinal Flatmounts

Laser exposed and uninjured transgenic and control mice were euthanized using cervical dislocation. Eyes were enucleated and fixed in 1% phosphate-buffered paraformaldehyde (PFA) for 1 hour. The neural retinas were extracted microsurgically from retinal flatmounts, whole-mounted on microscope slides, and fixed in mounting medium (DakoCytomation, Hamburg, Germany) for fluorescence microscopy. For cryosectioning, both eyes were enucleated from each mouse and were immediately embedded in Tissue-Tek optimal cutting temperature (O.C.T.) compound (Sakura Finetek, Torrance, CA), frozen in liquid nitrogen and stored at -80 °C. Microtome sections (6 μm) were cut through the entire retina, along the vertical meridian, on a cryostat at -20 °C and thaw-mounted onto Superfrost Plus glass slides (Fisher Scientific, Pittsburg, PA). Sections were then air-dried, fixed in cold acetone or 4% PFA for 10 minutes, stained with an anti-fade reagent with DAPI (Invitrogen Molecular Probes, Carlsbad, CA), and stored at -80 °C until fluorescence microscopy was performed (filter λ = 350 and 488 nm; model BXB1; Olympus, Tokyo, Japan).

2.5 Immunohistochemistry

Tissue sections were prepared as described above and anti-glial fibrillary acidic protein (GFAP), IBA-1, NeuN, CD65, and Glutamine Synthetase (GS) monoclonal antibodies (Genox, Baltimore, MD) were applied using standard biotin-streptavidin-base methods. Frozen sections were rehydrated through ethanol gradient and permeabilized with 0.1% Triton X-100 (Fisher Scientific, Pittsburgh, PA) in phosphate buffered saline (PBS)(Mediatech, Manassas, VA) for 10 minutes. Endogenous peroxidase activity was quenched with 3% hydrogen peroxide. Non-specific bind-

ing and incubation with primary antibody was performed using Vector Laboratories Mouse on Mouse (M.O.M. ™) kit. Primary antibody was incubated at 1:100 dilutions for 1 hour at room temperature. Secondary biotinylated antibody from the M.O.M. basic kit was diluted according to the manufacturer's instructions and incubated with the tissue for 30 minutes at room temperature. Afterwards, sections were incubated for 30 minutes at room temperature in avidin peroxidase conjugate, Vectastain Elite (Vector Laboratories, Burlingame, CA). Staining was achieved by using peroxidase substrate 3, 3'-diaminobenzidine (DAB)(Vector Laboratories) and the reaction stopped by washing the tissue in PBS.

2.6 TUNEL Assay

A biotin-streptavidin-based terminal deoxynucleotidyl transferase (TdT)-mediated deoxyuridine triphosphate nick end *in situ* labeling (TUNEL) kit (R&D Systems, Minneapolis, MN) was used. Retina tissue cryosections were permeabilized with 0.1% sodium citrate and 0.5% Triton X-100 (30 minutes at room temperature) and quenched with 3% hydrogen peroxide. Samples were then incubated at 37 ˚C with a mixture of TdT, deoxynucleotriphosphates conjugated to biotin, Mn^{2+}, and TdT reaction buffer for 1 hour. After the TdT reaction was stopped, the tissues were incubated 30 minutes at room temperature with streptavidin-conjugated horseradish peroxidase, washed with PBS, and developed with DAB substrate at room temperature.

2.7 Lesion Measurement and Statistics

The lesion areas detected in *in vivo* images were manually selected in ImageJ (National Institute of Health, Bethesda, Maryland) from scaled IR images of laser damage. The level of EGFP fluorescence associated with injury was measured using ImageJ. Areas of increased EGFP fluorescence associated with NF-κB transcription were manually traced using the freeform selection tool. The measured area, mean gray value, and integrated density (product of area and mean gray value) were recorded from each of the fluorescent regions of interest (ROIs). The mean pixel values of ten regions of each fluorescence image which did not contain EGFP fluorescence were averaged together and recorded as the average image background fluorescence value. The corrected total cluster fluorescence (CTCF) was calculated as the integrated density – (product of area of fluorescent cluster and mean background fluorescence).

A mixed model of repeated measures (SAS, Ver. 9.2; SAS Institute, Cary, NC) was used to detect any significant differences in CTCF versus grades of laser damage and observation time. Pearson's correlation was used to evaluate the relationship between CTFC and lesion area for suprathreshold damage.

3 RESULTS

3.1 Laser Induced Damage in the Mouse Retina

Slit lamp evaluation was used to assess successful delivery of laser exposures immediately after exposure. Multiple laser lesions were assessed in each subject. The hyper-reflective changes ranged from a "graying" of the exposed region to a blanched "white" appearance as exposure energy was increased. The minimal energy needed to produce a gray exposure was set as the threshold energy of 14.6 mW.

Figure 1 presents cSLO images of supra-threshold injury in a 1 year old wildtype mouse 24-72 hours after exposure. Autofluorescence baseline images of the retina appeared faint in younger mice (<3-4 months) in comparison to older mice used to help established injury thresholds (Figure 1C). There was an increase in autofluorescence of the retinal pigment epithelium (RPE) three days following laser exposure (Figure 1E). The evidence of the lesions in fluorescence angiography was used to help determine if RPE/Bruch's membrane was compromised by laser exposure (Figure 1D). Lesions were distinguishable 8-14 days in the RPE post exposure using 488 nm light whereas the lesions were no longer visible using the IR or RF imaging (not shown). Laser injury in the cis-NF-κB-EGFP mouse retina was similar to injury in the wildtype mouse. To distinguish EGFP measurements from autofluorescence of the retina, younger mice were selected for monitoring NF-κB *in vivo*.

OCT scans enabled a complimentary evaluation of lesion morphology to traditional *en face* imaging used to assess laser lesion dynamics and wound healing. No lesions were detected immediately following laser exposure but developed within the hour. Lesions identified in OCT B-scans were characterized as regions of hyper-reflectivity or hypo-reflectivity in comparison to surrounding retinal regions with visible disruption to the RPE and choroid.

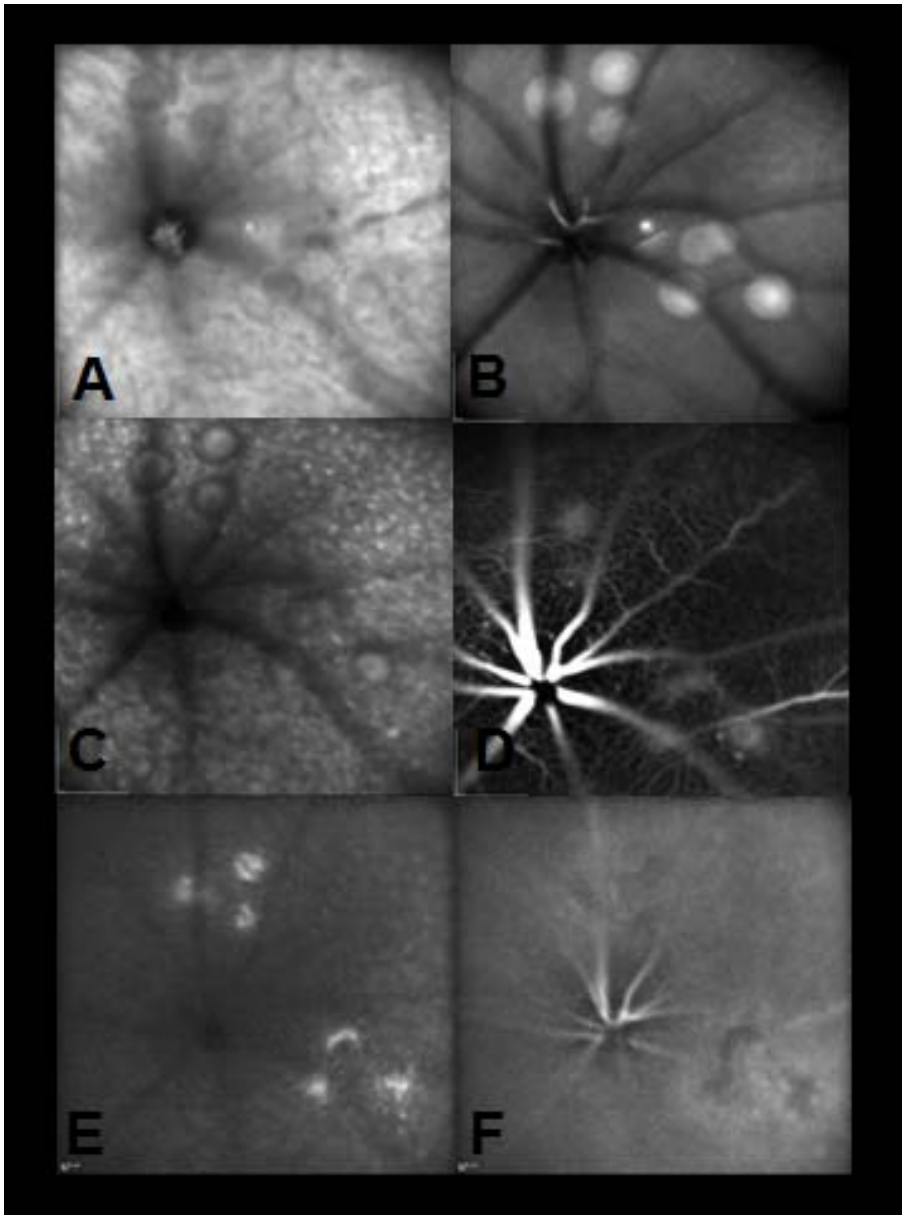

Figure 1: cSLO images (30° FOV) of supra-threshold laser lesions in a 1 year old wildtype mouse retina 24 (A-D) and 72 hours (E-F) post exposure. (A) Infrared, (B) red-free, (C and E) autofluorescence (488 nm), (D) fluorescein angiography, and (F) indocyanine green imaging modalities

Figure 2 shows FA and OCT images of a supra-threshold lesion in a wildtype mouse 1 and 24 hours after initial exposure. One hour following laser exposure, disruption to the RPE/Bruch's membrane appeared as regions of hypo-reflection in the RPE into the photoreceptor layer (Figure 2A). Figure 2B shows an FA image of the same lesion and location of the B-scan in Figure 2A (green line). The areas of hypo-reflection changed into a region of hyper-reflectivity extending from the outer retina into the choroid at the 24 hour observation point (Figure 2C). Disruption of the RPE/Bruch's membrane visible immediately after laser exposure (Figure 2B) was not always evident at the 24 hour follow up (Figure 2D).

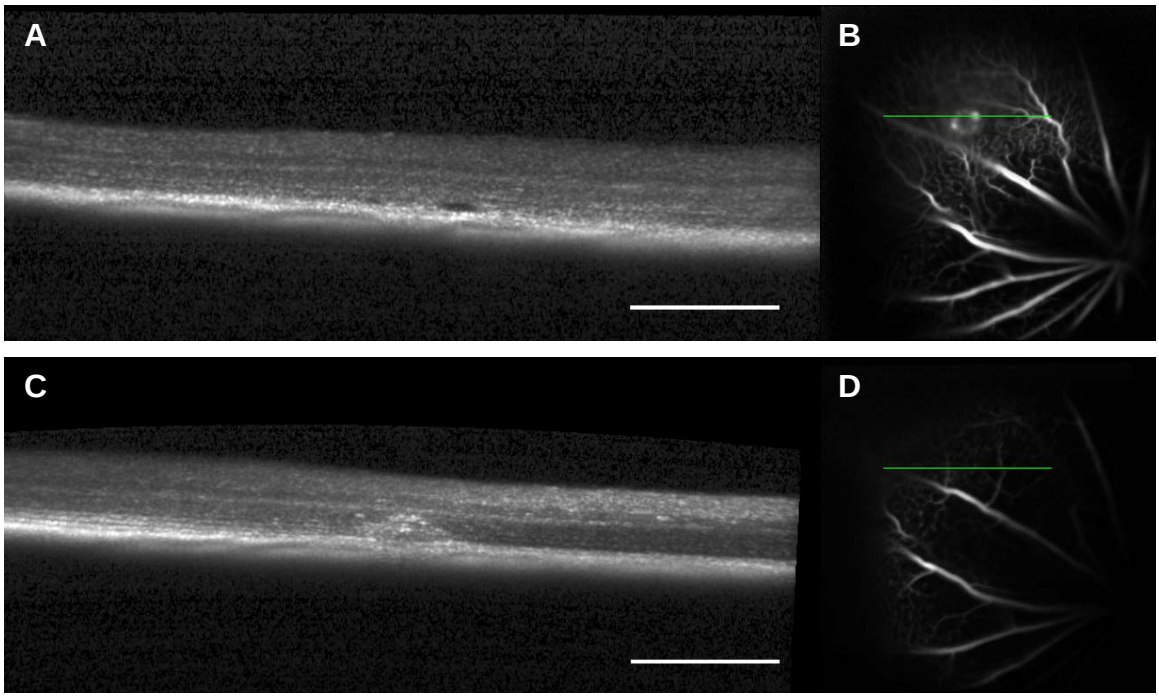

Figure 2: (A) OCT and (B) FA image (30° FOV) of mouse retina immediately following thermal laser injury. Follow up OCT (C) and FA image (D) of same subject 24 hours later (30FOV). Scale Bar: 100 µm (x-axis)

Lesion size metrics were collected from a subset of wildtype and transgenic mice for association with the magnitude of EGFP protein expression indicative of NF-κB activation. Discernible lesion areas for subjects which received supra-threshold exposures were measured from infrared cSLO images (Figure 3). Lesion width and area was measured with a single B-scan in the raster set where the damage was greatest based on visual inspection for subjects receiving threshold exposures (Figure 4).

Injury was localized to the outer retinal layers for all grades of visible laser damage. Infrared images collected within four hours of threshold and supra-threshold exposures appeared as hyporeflective regions with a hyper-reflective "ring" surrounding the lesion circumference (Figure 3A). Laser exposures less than 8.4 mW did not produce any visible lesions. Threshold lesions "resolved" faster than supra-threshold lesions as they were not apparent in infrared images collected 5 days after exposure. Supra-threshold lesions (n=51) grew 26% bigger 48 hours following exposure (Figure 5). Threshold lesions decreased in width 20% from 24 to 48 hours following exposure (Figure 6). Lesion size continued to decrease for both grades of injury for each observation point past 48 hours.

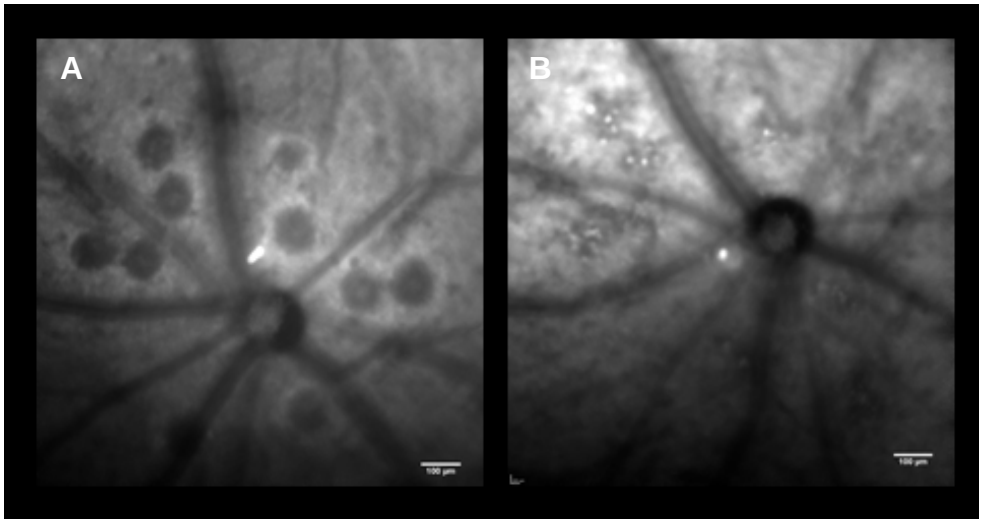

Figure 3: Supra-threshold injury in transgenic mouse (A) 4 hours (B) 7 days. Scale Bar: 100 µm (x-axis)

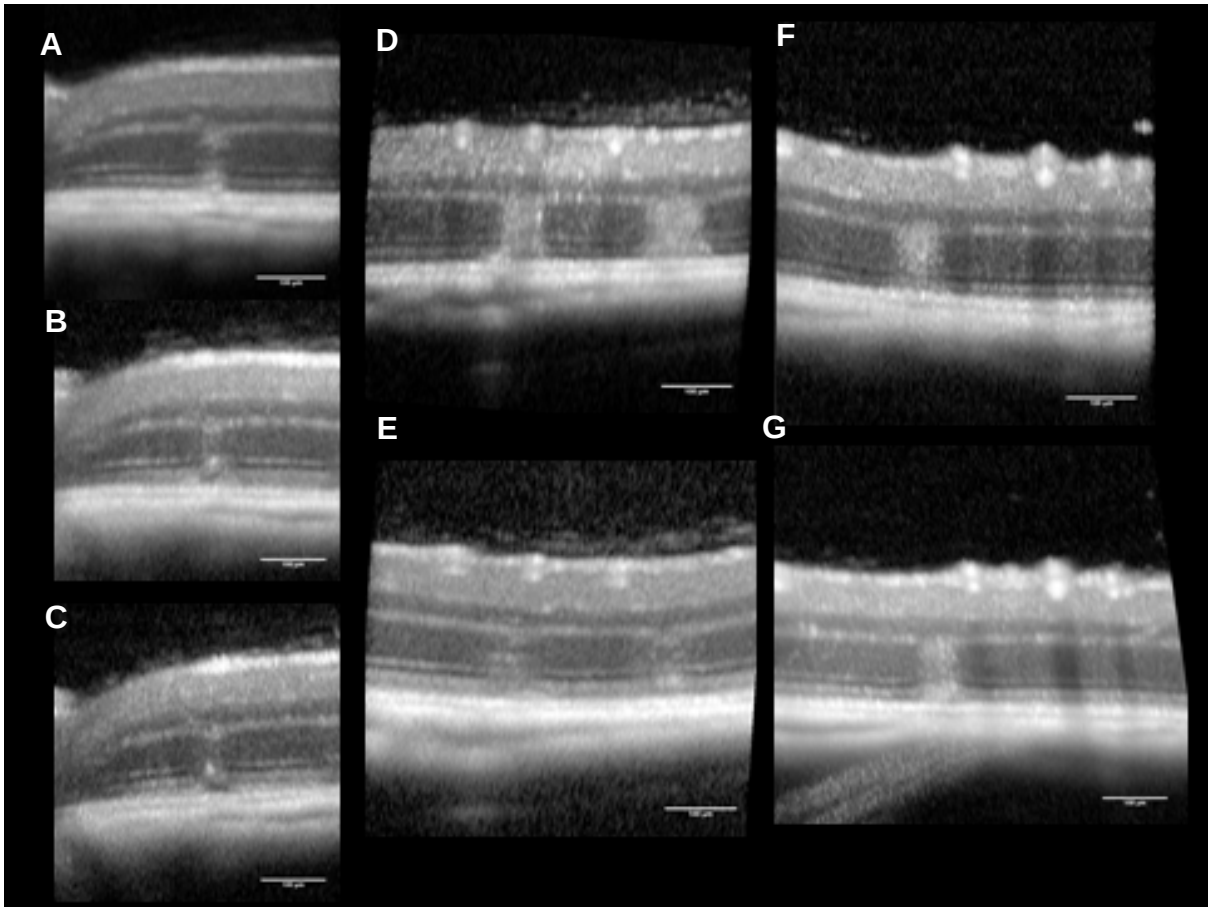

Figure 4: OCT B-scans of threshold injury exposure in three cis-NF-κB-EGFP mice (A-C) Top to bottom: 24 hours, 5 days, and 7 days post exposure. (D-E) Top to bottom: 24 hours and 5 days post exposure. (F-G) Top to bottom: 24 hours and 48 hours post exposure. Scale Bar: 100 µm (x-axis)

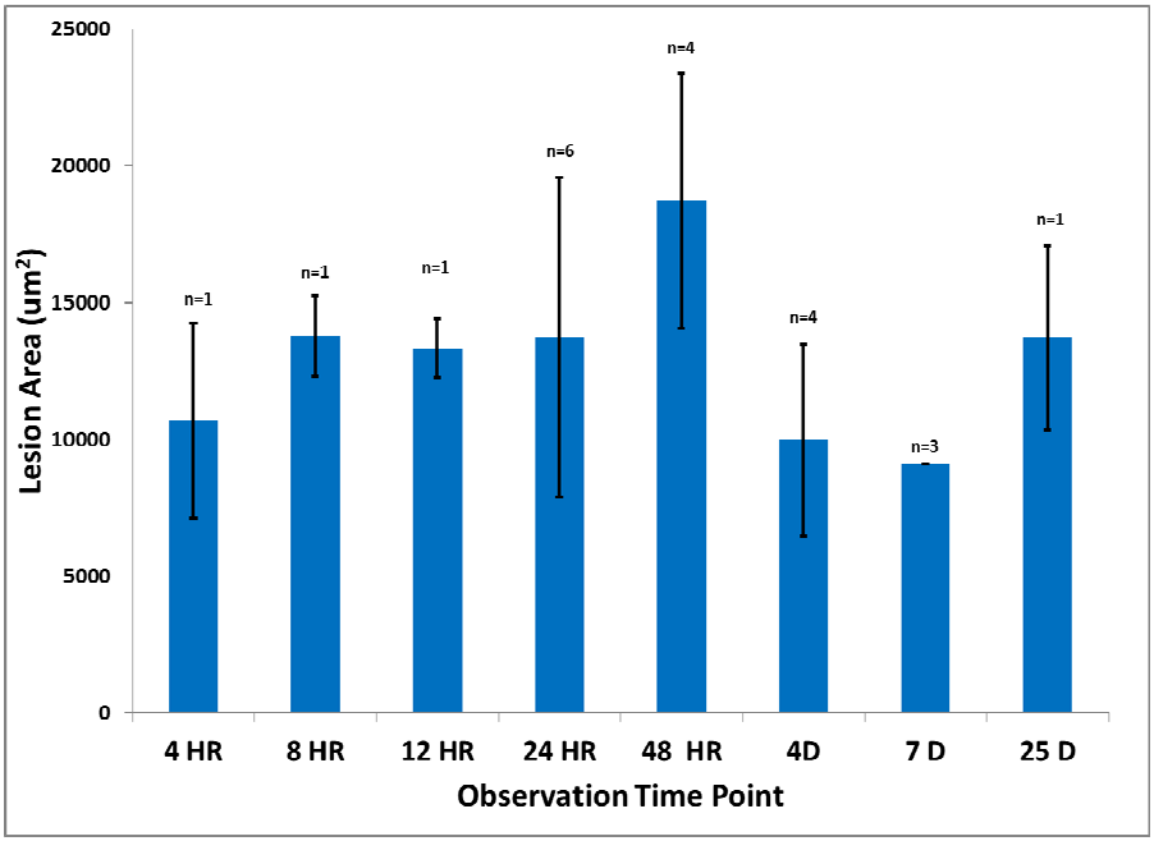

Figure 5: Average lesion area measurements collected from infrared images of cis-NF-κB-EGFP mice (n=6) retinas which received supra-threshold exposures. The number of mice included in each measurement is above each respective bar.

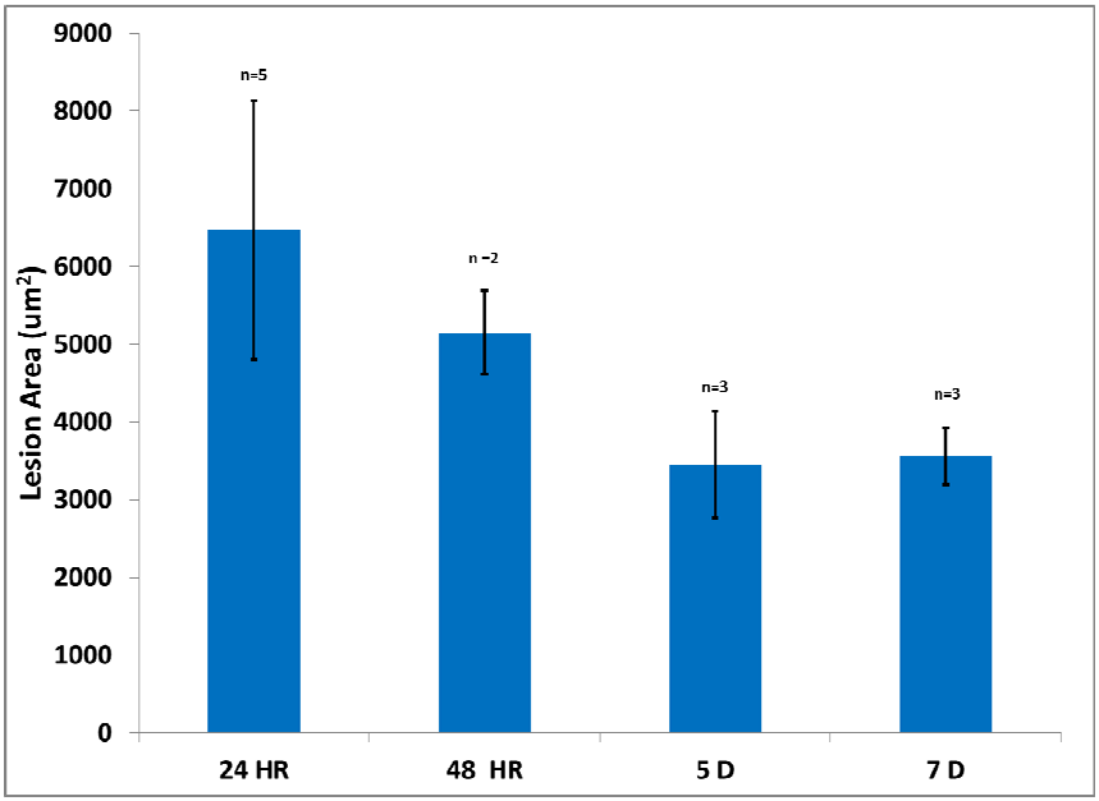

Figure 6: Average lesion area measurements collected from OCT B-scans of cis-NF-κB-EGFP mice (n=5) retinas which received threshold exposures. The number of mice included in each measurement is above each respective bar

3.2 Basal Expression Pattern of cis-NF-κB-EGFP Transgene

3.2.1 cSLO Imaging.

Baseline fundus photos collected using cSLO with an excitation wavelength of 488 nm allowed study of basal expression of NF-κB associated with translocation to the nucleus. Reflectance and fluorescence images were collected with focus setting ranging from -10 to 10 diopters to examine signal depth dependence within the retina (Figure 7). The fluorescent structures associated with the retinal vasculature were best focused at retinal positions slightly posterior to the nerve fiber layer (Figure 8).

Fluorescence emanating from the anterior retinal vasculature close to the nerve fiber layer was a distinguishing characteristic observed in most cis-NF-κB-EGFP mouse retinas. EGFP fluorescence intensity and expression patterns associated with NF-κB (p65) transcription were unique to each mouse (Figure 9).

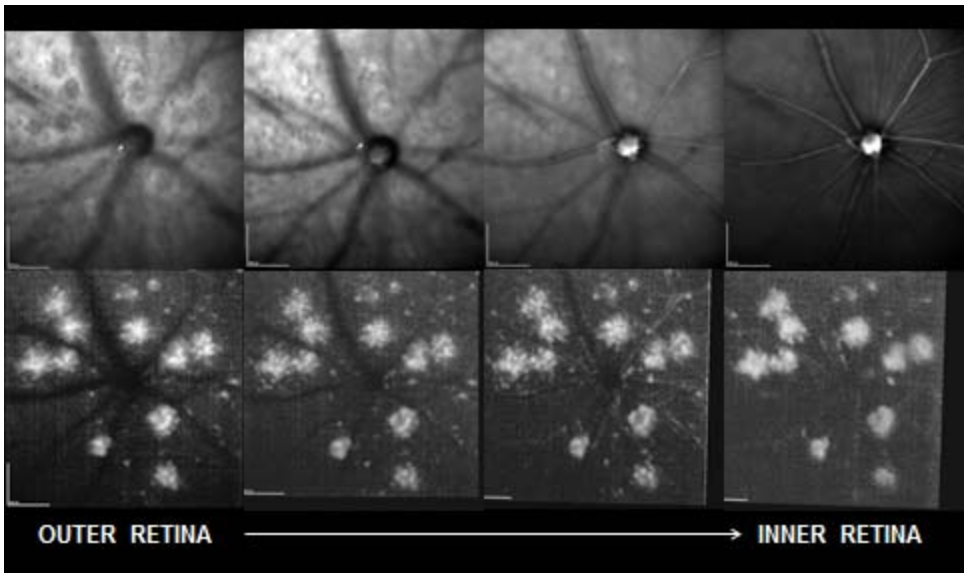

Figure 7: Infrared (top row) and complimentary fluorescence images (bottom row) from cis-NF-κB-EGFP mouse 48 hours following laser exposure. Focus settings from left to right: -10 diopter (outer retina), -5 diopter, 0 diopter, and 5 diopter (focused on nerve fiber layer). Scale Bar: 200 µm

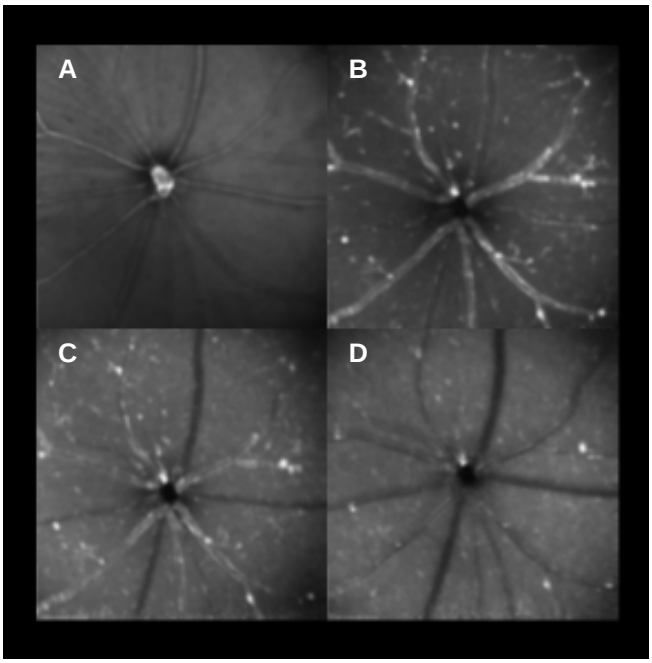

Figure 8: Fluorescence and infrared SLO images (30º FOV) of a single cis-NF-κB-EGFP mouse retina. (A) Infrared image with focus setting at -5 diopters slightly posterior to the nerve fiber layer. (B) Fluorescence image with focus held at -5 diopters. (C) Fluorescence image with focus posterior to figure B (0 diopters). (D) Fluorescence image with focus setting at +5 diopters

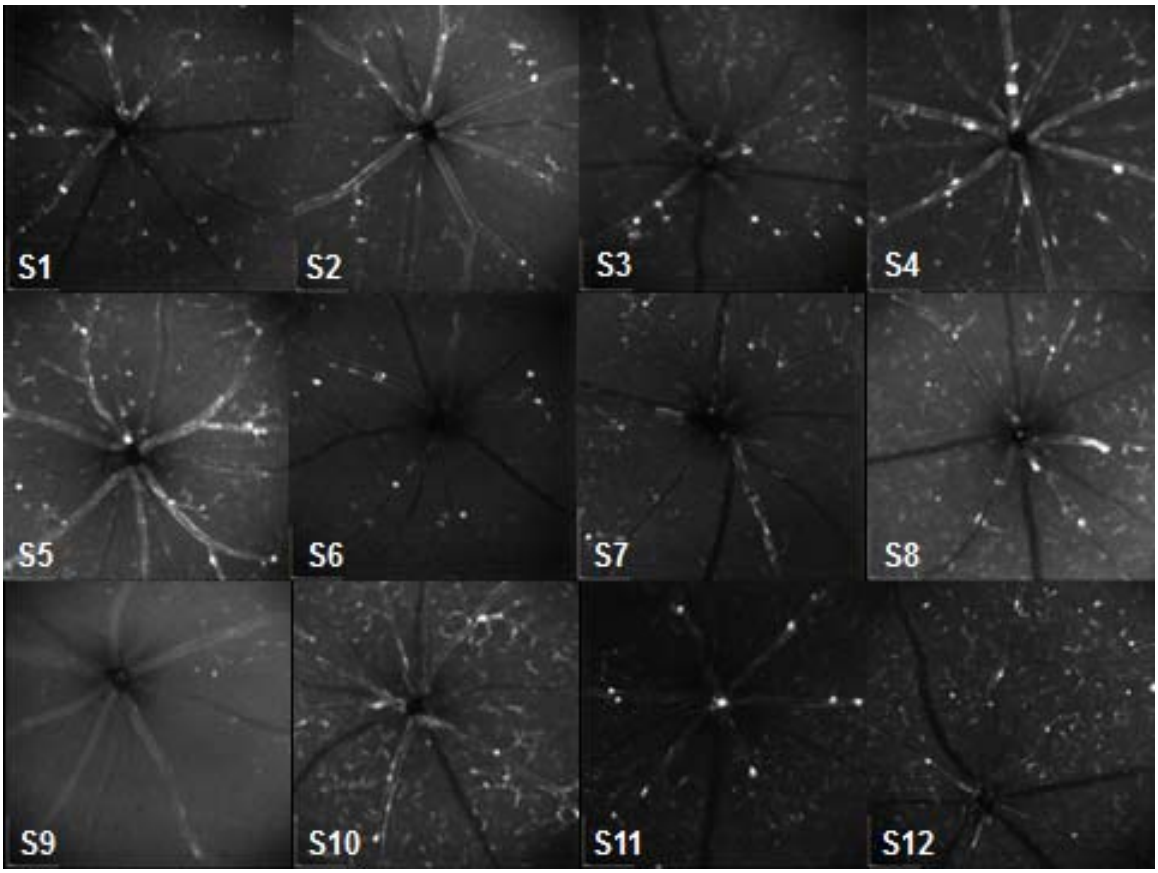

Figure 9: Fluorescence images of 12 uninjured cis-NF-κB-EGFP mouse retinas

A fluorescent population of cells were seen circulating in the retinal fundus, but the cell type is not clear (Figure 10). The peripheral mononuclear cells of the cis-NF-κB-EGFP mouse are EGFP+ are a likely cell population. The time between each of the frames in Figure 10 is 66 ms. Tracking EGFP+ cell bodies from a movie collected four hours after supra-threshold laser injury in one subject (Figure 10 and 11), the calculated average velocities were 0.99±0.22 mm/s, 0.22±0.06 mm/s, and 0.74±0.42 mm/s, respectively. Summary of a sampling of cell velocities are given in table 2. Some of the EGFP+ cell bodies (cell numbers 4-7) travel a greater distance in a shorter time and could only be captured within two consecutive frames (~3.73 mm/s). Figure 10 shows the retina fundus before injury (A), four hours (B), and 24 hours later (C). Two EGFP+ cells are highlighted in red in the single frame in Figure 10B.

Table 2: Sampled measures of EGFP+ cell velocities

EGFP Cell Number	Measure 1	Measure 2	Measure 3	Measure 4	Average Velocity (mm/s)
1	1.15	0.81	0.75		0.90
2	0.24	0.29	0.20	0.15	0.22
3	1.03	0.26	0.94		0.74
4	3.50				
5	3.34				
6	4.48				
7	3.60				

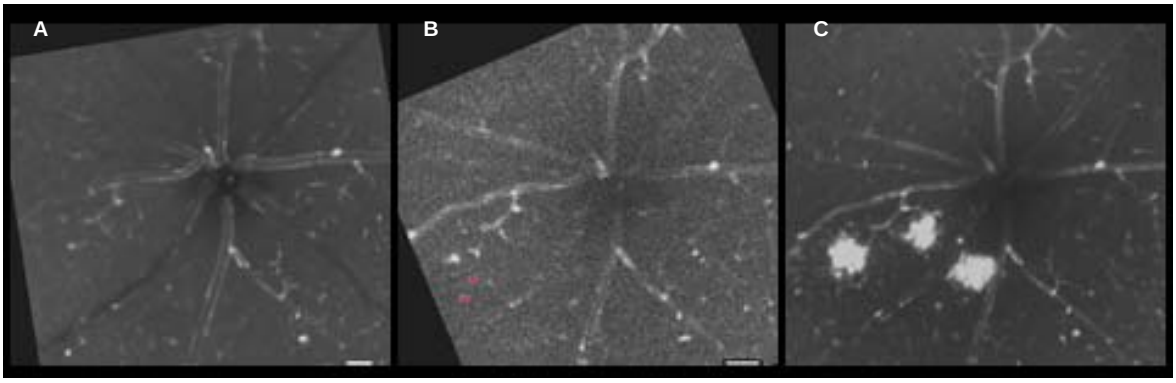

Figure 10: Infrared and fluorescence images (30 FOV°) of cis-NF-κB-EGFP mouse before and after supra-threshold exposures. All images are co-registered to the same rotational orientation. (A) IR fundus before injury. (B) Fluorescence image of injured retina four hours following injury. Two EGFP+ cells are highlighted in red. (C) Fluorescence image of the same injured retina 24 hours later. Scale bar: 100 µm

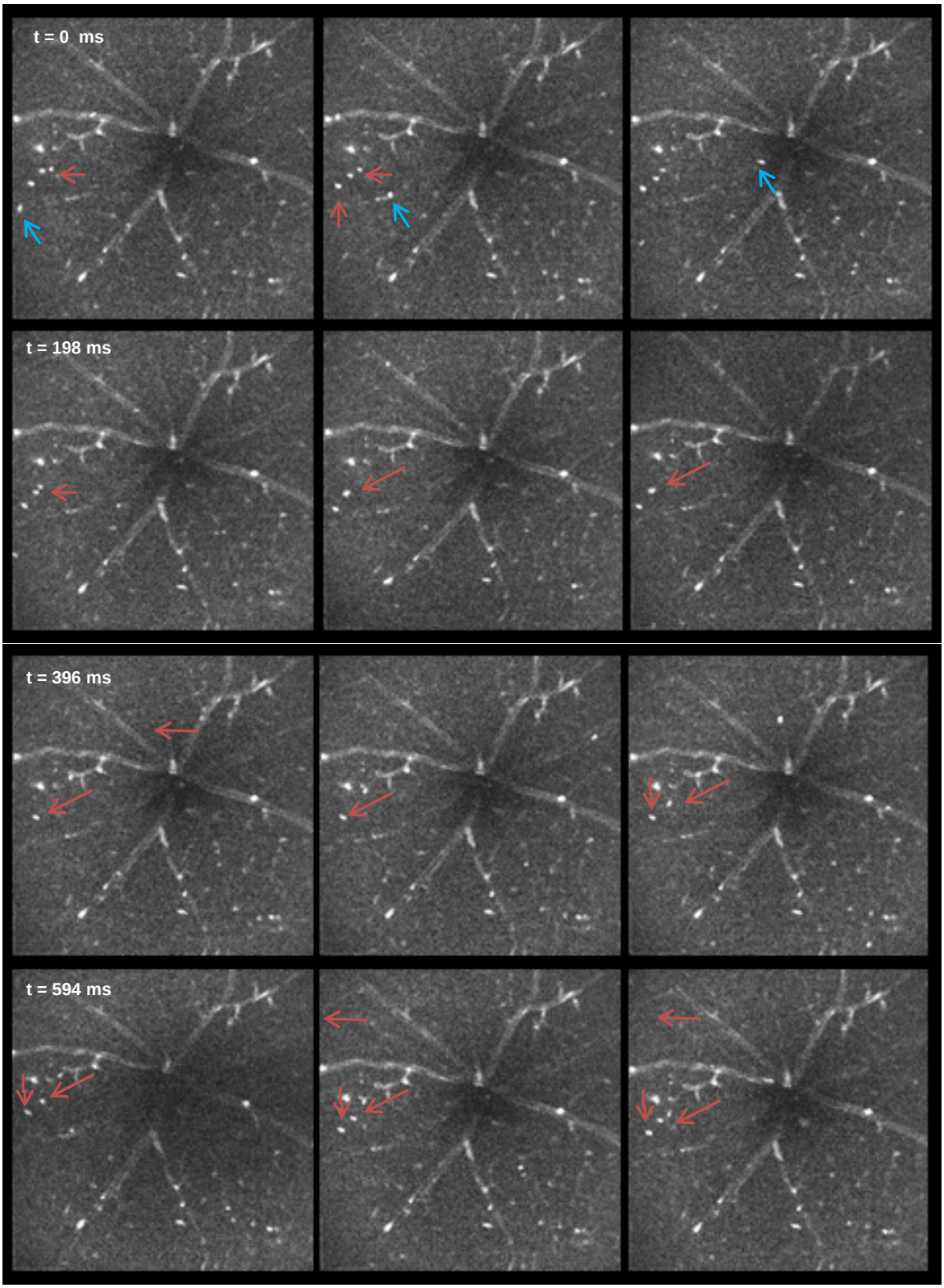

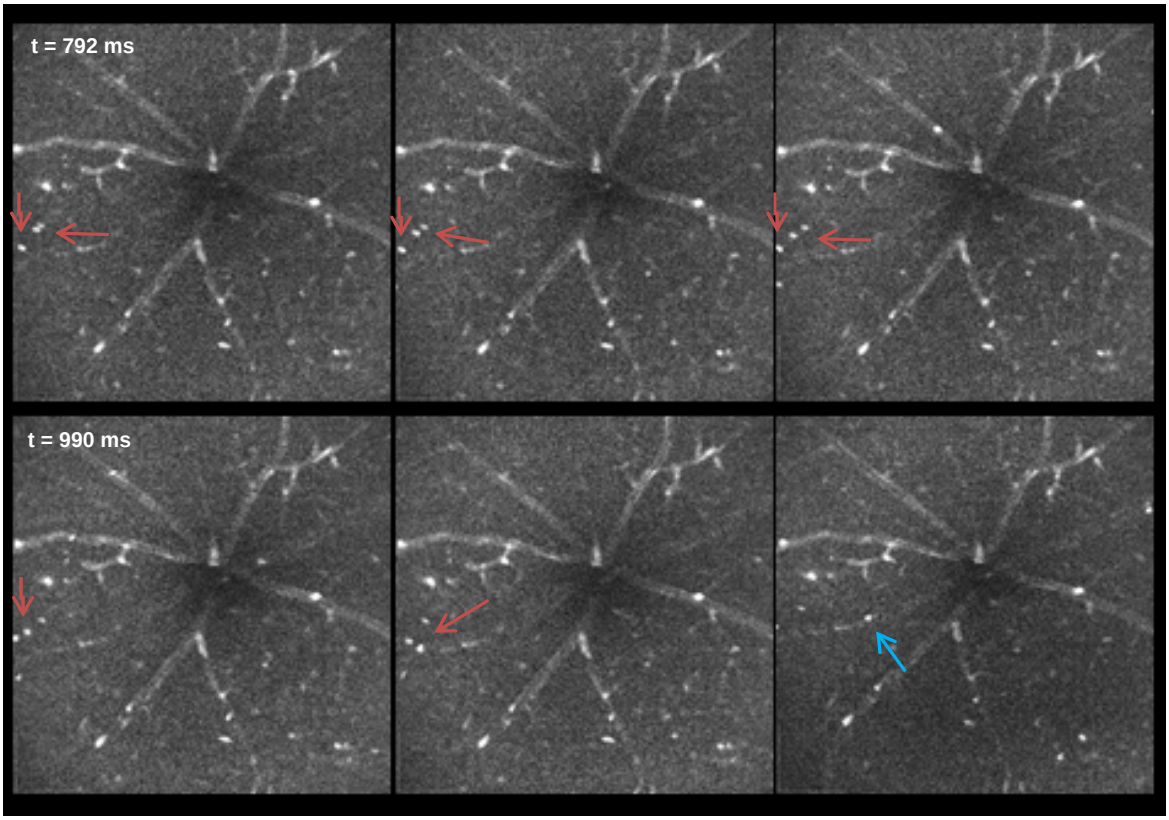

Figure 11: Fluorescence image single frames (30º FOV) collected four hours after supra-threshold injury of a cis-NF-kB-EGFP mouse retina. The red arrows point to a location in the retina where the EGFP+ cells "collect" before exiting the region via major blood vessels (blue arrows). The time in ms between every three frames is given in the top left corner

3.2.2 Fluorescence Microscopy

Retinal flatmounts and cryosections of uninjured and injured retinas of the cis-NF-κB-EGFP mouse were analyzed to examine constituent expression patterns and localization of NF-κB (p65) to further characterize the EGFP signal seen in fluorescent cSLO images. Figure 12 below is an example of a retinal flatmount and cryosection from the cis-NF-κB-EGFP mouse retina. Retinal flatmounts confirmed the retinal vasculature as a source of the EGFP signal within the retina. NF-κB expression was present within the retinal ganglion cells (RGC), inner plexiform layer (IPL), and outer plexiform layer (OPL) as seen in cryosections of the retina (Figure 12B). Most of the EGFP+ signal seen within the RGC layer was adjacent to retinal blood vessels.

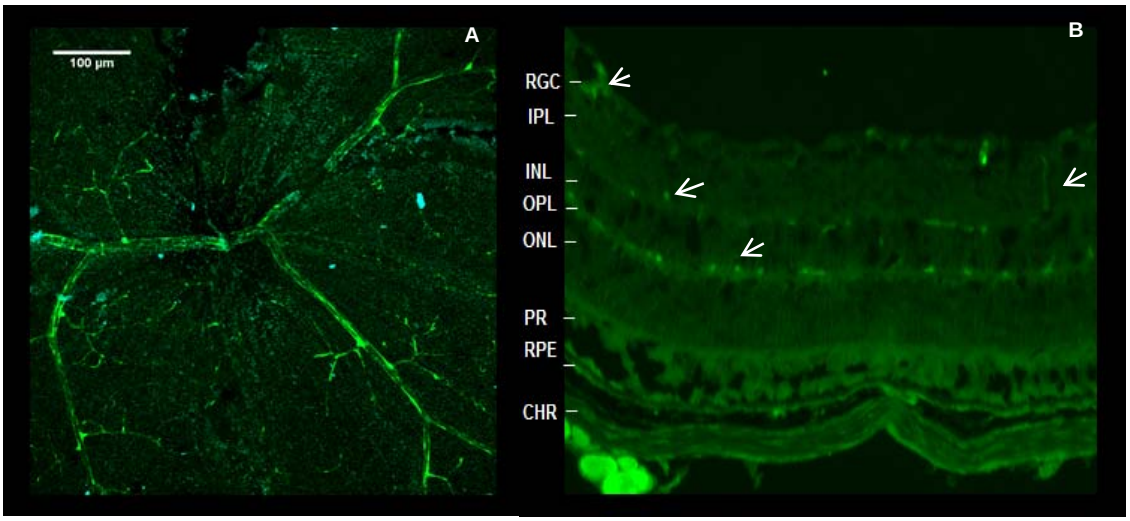

Figure 12: (A) cis-NF-κB-EGFP retinal flatmount stained with DAPI. (B) Fluorescence microscopy (green channel) of a retinal cryosection from an uninjured mouse. NF-κB (p5) localization can be seen in the RGC, IPL, and OPL (white arrows). A "string" like structure resembles a Müller process. (far right arrow)

Cryosections were stained with DAPI, IBA-1, GFAP, and NeuN to help identify specific cell bodies and/or retinal structures constituently expressing the p65 NF-κB protein. None of the complimentary stains co-localized with the EGFP signal. DAPI stain is specific to the nuclear regions of cell bodies and preferentially stains the ganglion cell layer (GCL), inner nuclear layer (INL), and outer nuclear layer (ONL) of the retina (Figure 13B). Amacrine and ganglion cells were stained with the NeuN antibody tagged with red fluorescent protein (Figure 13D). Activated microglial and Müller cells expressing the IBA-1 (Figure 13B) and GFAP protein (not shown) respectively were also eliminated as co-localizing with EGFP+ structures.

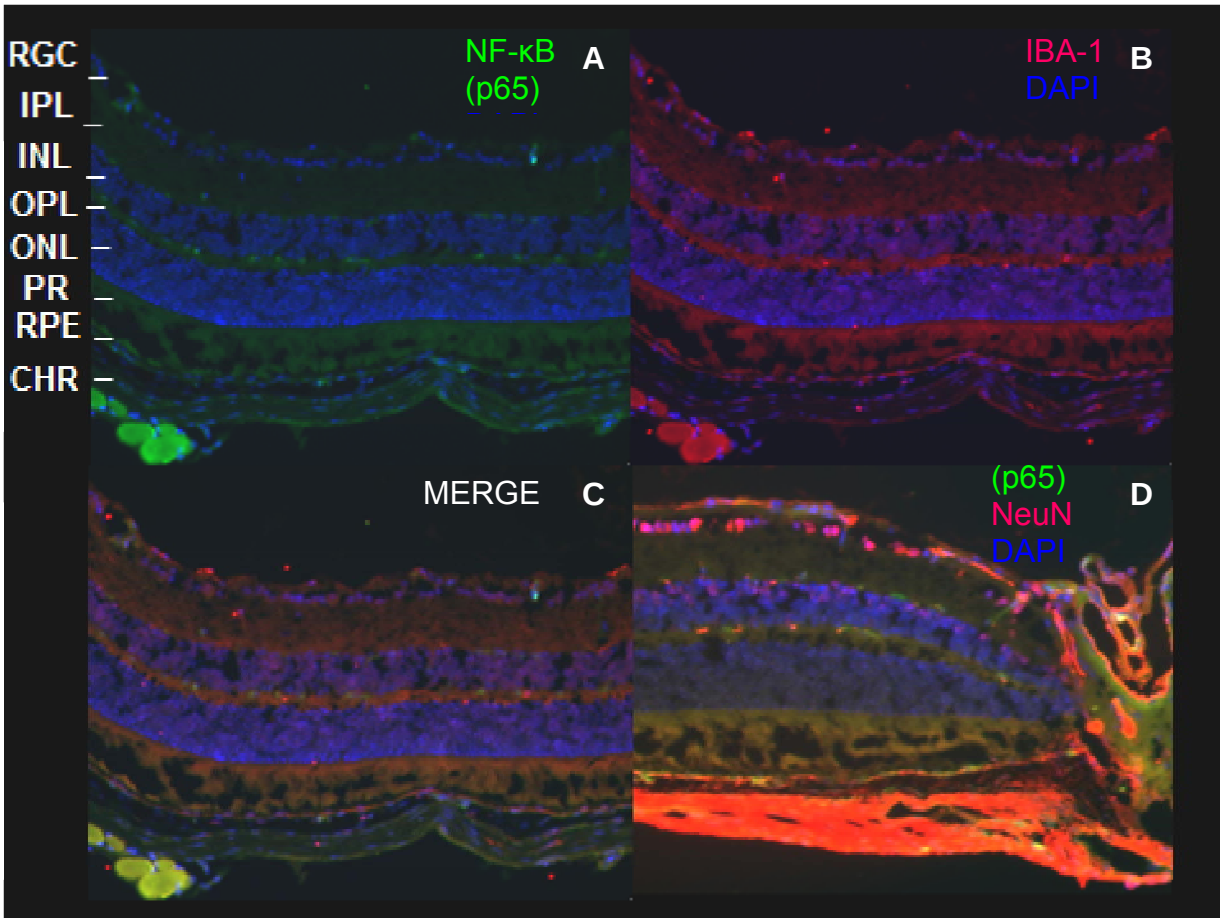

Figure 13: Immunofluorescence labeling of retinal cryosections of cis-NF-κB-EGFP (uninjured) (A) EGFP overlaid with DAPI stain. (B) Double immunofluorescence staining with IBA-1 (red) and DAPI (blue). (C) Merger of figures A and B. (D) Double immunofluorescence staining surround the optic nerve head with NeuN (pink), DAPI (blue), and EGFP+ structures (green)

3.2.3 Two-photon Imaging.

Two-photon and reflectance imaging of an uninjured retina revealed most of the EGFP+ signal co-localized within the inner retinal layers. Figure 14 shows two-photon sectional *en face* images of a non-injured cis-NF-κB mouse retina. The nuclear region of the INL cell bodies has constitutive expression for this subject (white arrow).

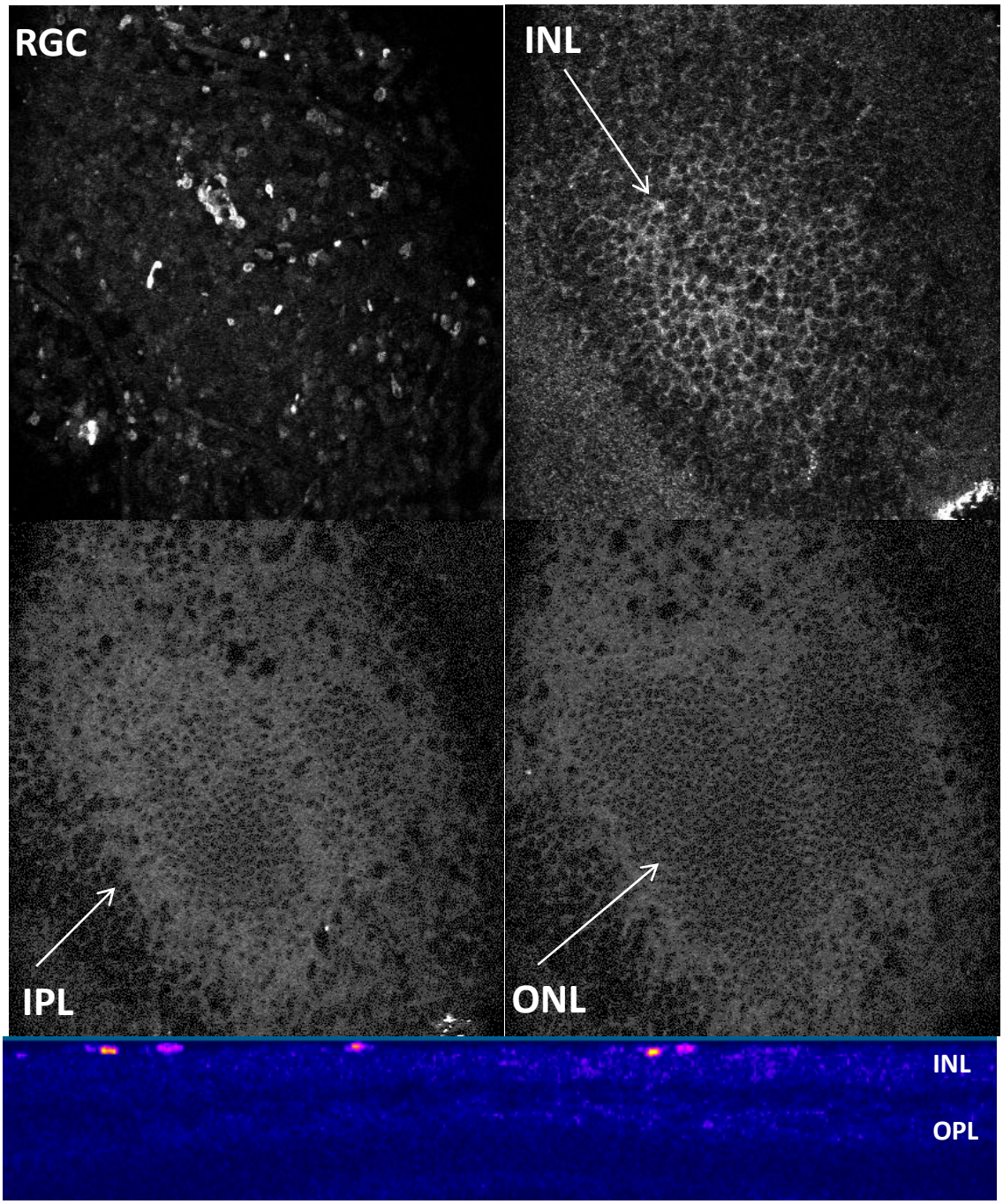

Figure 14: Two-photon images of cis-NF-κB-EGFP mouse retina ex-vivo. Two-dimensional enface view of the retina starting with the RGC (Top left) and ending with the ONL (Middle right). (Bottom) Cross-sectional slice of three dimensional volume demonstrating hyperfluorescent regions in the inner retina

3.3 Expression Pattern of cis-NF-κB-EGFP Transgene Following Laser Injury

3.3.1 *In Vivo* cSLO Imaging.

In vivo imaging allowed monitoring of the spatial and temporal activation of NF-κB following laser injury in the murine retina. Mice receiving only the imaging treatment without laser expo-

sure did not show any activated EGFP fluorescence (data not shown). Sub-threshold exposures did not produce visible lesions or activate EGFP (data not shown). Retinal regions exposed to threshold and supra-threshold laser damage produced fluorescent cell "clusters" minimally 4-6 hours later. EGFP expression associated with threshold and supra-threshold exposure was variable between mice and also variable within the same mouse. The best focus of the fluorescent clusters was anterior to the RPE and beneath the nerve fiber layer.

Fluorescence intensity of the supra-threshold regions increased over the 24-48 hour period as the "clusters" became more uniform in appearance compared to a mottled appearance at 24 hours (Figure 15). Fluorescence cluster intensity peaked at 48 hours and began to degrade thereafter (Figure 16). NF-κB expression associated with fluorescence was variable on the fifth observation day with an increase of some portions of the fluorescent "clusters" without an increase in size. Fluorescence intensity indicative of NF-κB transcription (CTFC) was grouped and averaged for all mice receiving supra-threshold treatment (n=146 lesions).

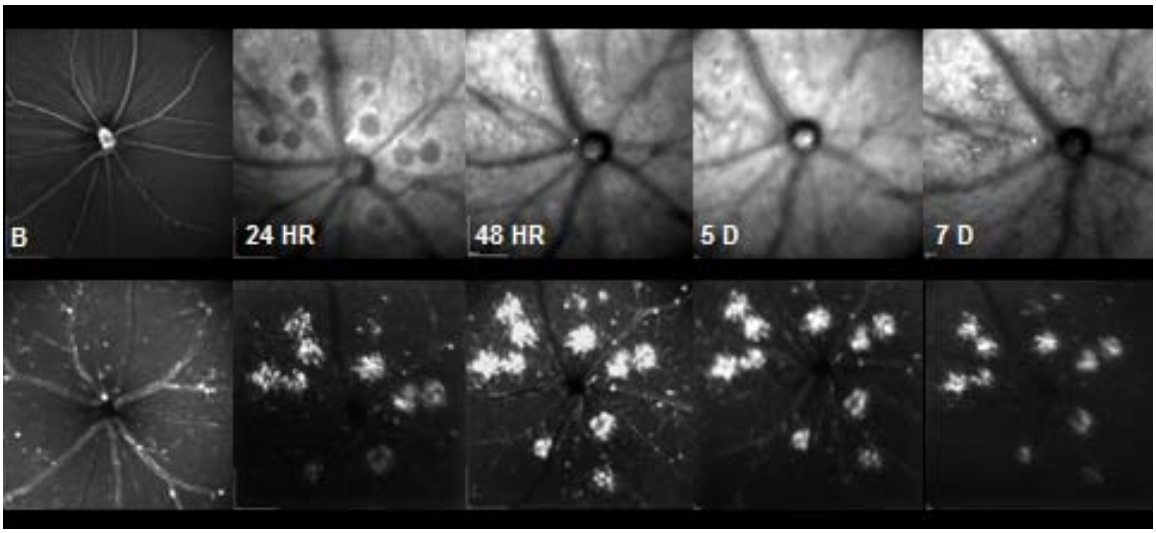

Figure 15: Baseline (B) and follow on infrared (top row) and complimentary fluorescence images (bottom row) from cis-NF-κB-EGFP mouse 24 hours to 7 days following supra-threshold laser exposure

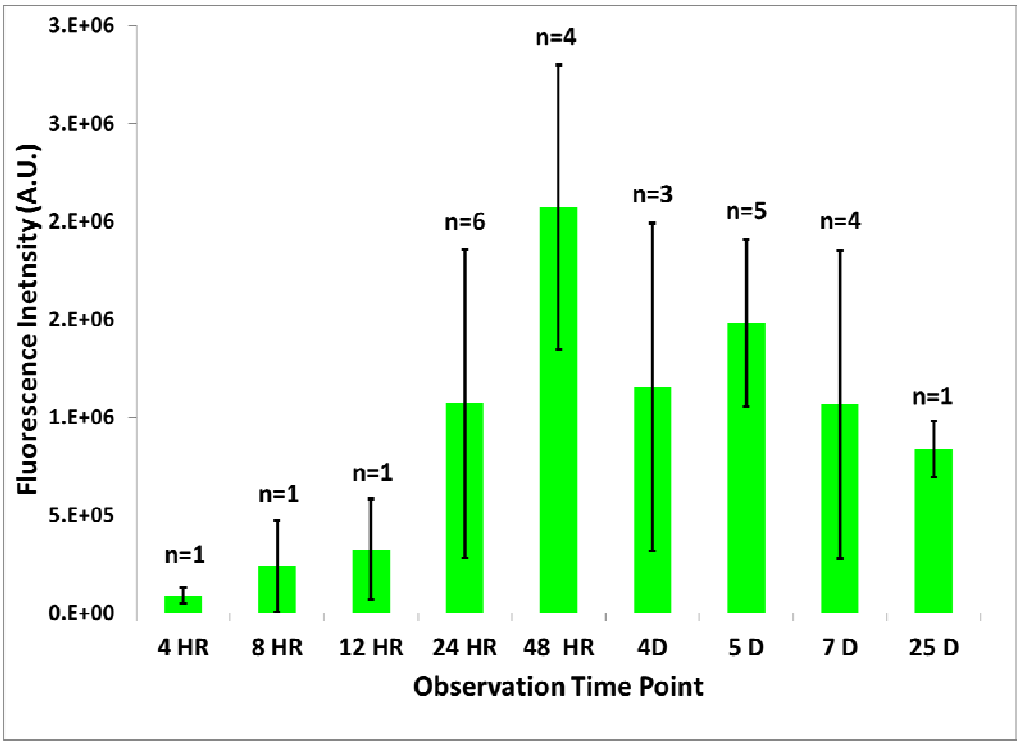

Figure 16: Summary of mean EGFP fluorescence (arbitrary units) supra-threshold lesion clusters indicative of NF-κB transcription. The number of animals included in each measurement is indicated above each respective bar

Threshold injury CTFC had a similar appearance to the fluorescent clusters of supra-threshold damage but occupied a smaller area (Figure 17) and had less fluorescence (Figure 18). Fluorescence intensity indicative of NF-κB transcription was grouped and averaged for all mice receiving threshold treatment (n=66 lesions) based on exposure day. Lesion fluorescence was maximal at 24 hours and decreased at each following observation point thereafter (Figure 18).

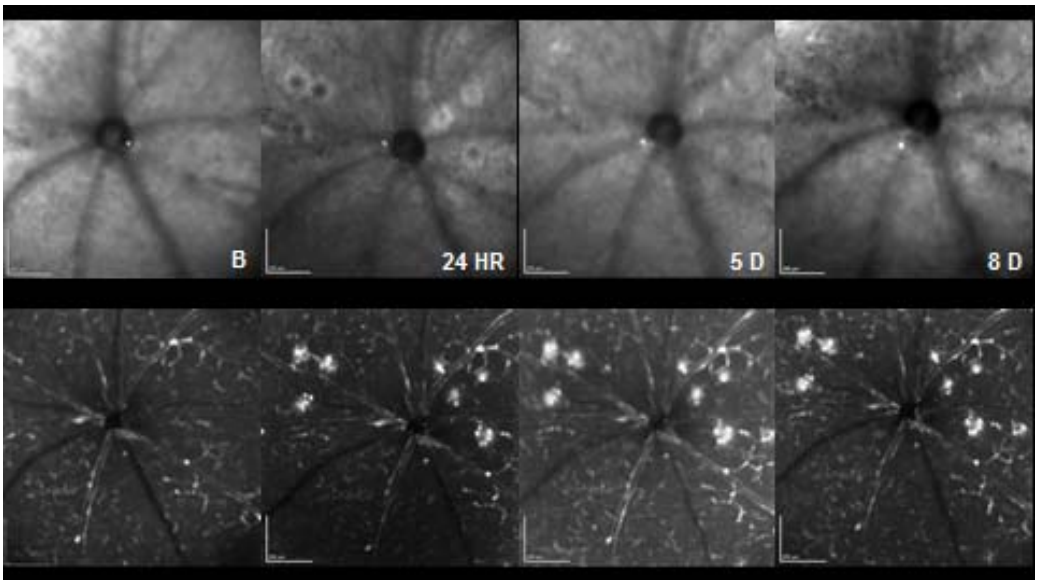

Figure 17: Baseline and follow on infrared (top row) and complimentary fluorescence images (bottom row) from cis-NF-κB-EGFP mouse 24 hours to 7 days following threshold laser exposure. Scale Bar: 200 µm

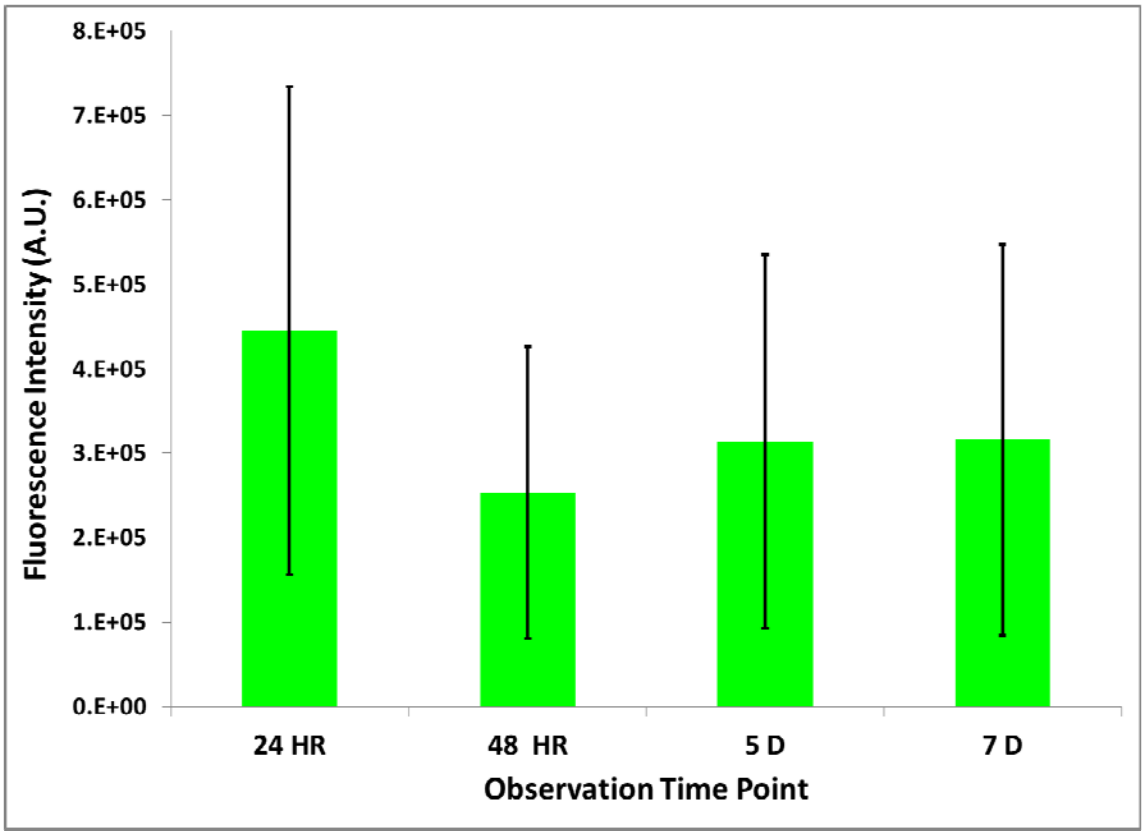

Figure 18: Summary of mean EGFP fluorescence of threshold injury fluorescent lesion clusters indicative of NF-κB transcription. The number of animals included in each measurement is indicated above each respective bar

A two level mixed effects model of repeated measures was used to compare the fluorescence clusters resulting from the two grades of laser damage for matched time points (24 hours, 48 hours, 5 days, and 7 days) for respective mice (Figure 19). The null hypothesis compares the differences in the variance by allowing variances to vary by time and mouse versus keeping the variance fixed. The null hypothesis is: H_0: $(\sum \sigma^2 I) = N(0, \sigma^2 I)$ versus H_1: $(\sum \sigma^2 I) \neq N(0, \sigma^2 I)$, where ($I$) is the identity matrix of dimension equal to the number of subjects.

H_0: There is no difference in the variance allowing the interaction to vary by time and by mouse $(\sum \sigma^2 I)$ and does not account for any more variance in comparison to being fixed $N(0, \sigma^2 I)$.

H_1: There is a difference in variance allowing the interaction to vary by time and by mouse $(\sum \sigma^2 I)$ and does account for any more variance in comparison to being fixed $N(0, \sigma^2 I)$.

The null model likelihood ratio test rejects the null hypothesis with a Chi-Square value of 4.0 and is significant (P<0.04). The second order mixed effects model for the data is:

$$Y_{ijk} = u + \alpha_i + \gamma_k + (\alpha\gamma)_{ik} + e_{ijk} \qquad (1)$$

where Y_{ijk} is the dependent variable of the fluorescence measurement at each time k for the j^{th} mouse assigned to laser treatment i. The right hand side of equation (1)

$$u + \alpha_i + \gamma_k + (\alpha\gamma)_{ik} + e_{ijk} \qquad (2)$$

is the mean for laser exposure grade i at time k, containing effects for laser exposure grade, time, and the product of laser exposure grade and time interaction. The random error associated with the measurement Y_{ijk} is e_{ijk}. The results of the model indicate there is a significant effect of laser dose on the amount of fluorescence (NF-κB transcription) resulting from injury (P=0.006), and there is a marginal effect of the amount of fluorescence (CTFC) at the time of evaluation (P=0.055). There was a significant interaction between the product of observation time and laser dose (P=0.03). Overall, the exposure irradiance of visible lesions dictated the level of fluorescence (indicative of NF-κB transcription) detected as well as the duration of expression.

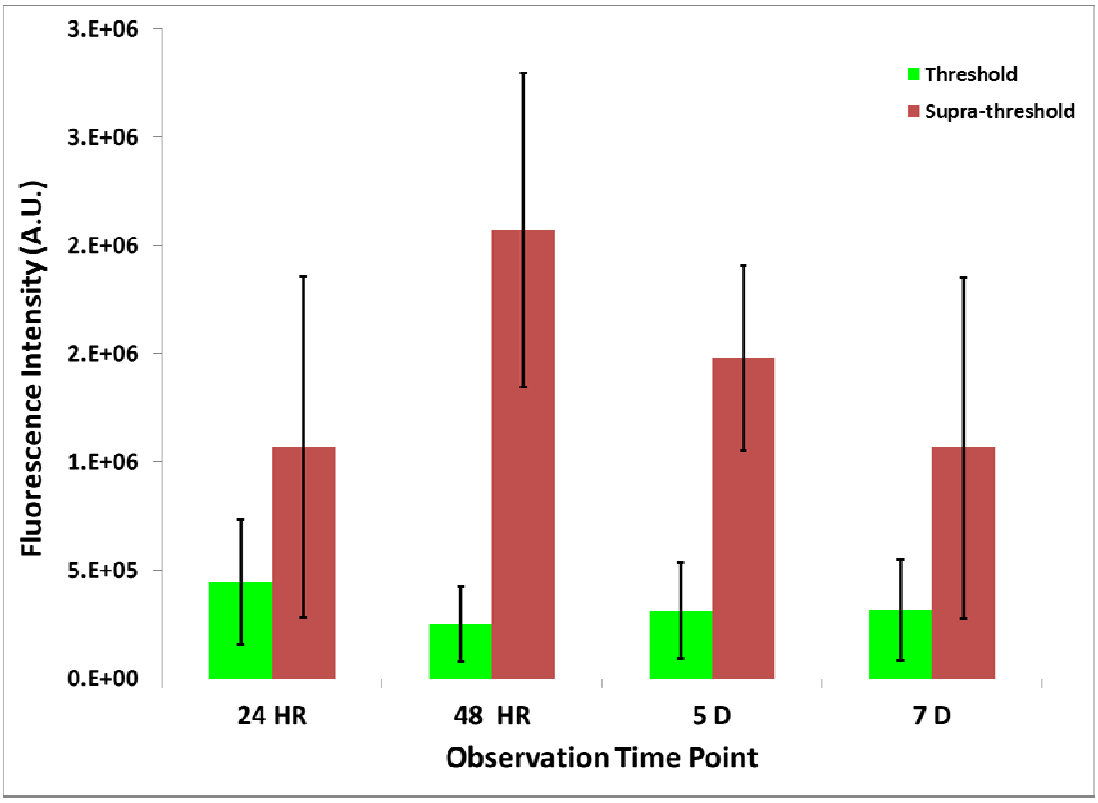

Figure 19: Comparison of supra-threshold and threshold exposures for mice evaluated at time matched observation points

Figure 20 depicts fluorescence images with complimentary OCT volume scans, collected to compare fluorescence intensity against lesion size at 24 hours and 5 days. Average lesion area increased over a 48 hour period for subjects receiving supra-threshold exposures. There was a weak but significant correlation (r =0.29, P=0.0017) between supra-threshold lesion size and EGFP fluorescence indicative of NF-κB transcription. Average threshold lesion size decreased gradually from its peak at 24 hours.

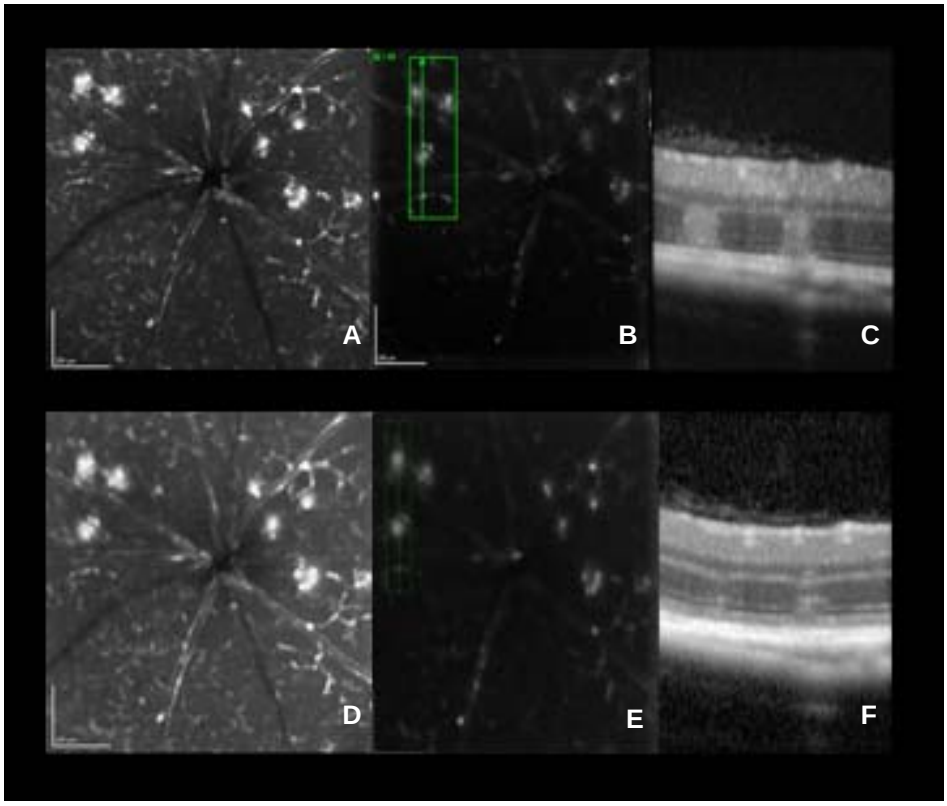

Figure 20: OCT and fluorescence images were simultaneously collected to examine fluorescence intensity in relation to lesion size. (Top row) (A) High quality fluorescence image captured 24 hours following laser exposure with (B) fluorescence image depicting OCT scan position. (C) OCT scan of lesions 24 hours later. (Bottom) (D) High quality fluorescence image captured 5 days following laser exposure with (E) fluorescence image depicting OCT scan position. (F) OCT scan of lesions depicted in row above 5 days later. Scale Bar: 200 µm

3.3.2 Fluorescence Microscopy and Immunohistochemistry of Retinal Flatmounts and Cryosections of Injured Retina.

Confocal fluorescence microscopy of *ex vivo* neural retinal flatmounts 3 and 10 days post supra-threshold retinal injury revealed a dense network of fluorescent interconnected cell bodies extending the full width of the neural retina. Figure 21 shows fluorescence stack images (focused at the anterior portion of the retina) of supra-threshold injury with (B) and without DAPI staining (A). The images were collected ten days following laser insult. The EGFP expressing cell bodies in the stack images have a similar appearance to the fluorescent "clusters" in the *in vivo* fluorescence images captured from the same subject (Figure 21C, D, and E).

Figure 22 shows confocal images of a DAPI stained flat mounted retina (with RPE removed) of a supra-threshold lesion 3 days post injury. Most of the EGFP expressing cell bodies are located with the ONL and OPL and with some in the RGC layer (cross-sectional view Figure 22 (Right)). *En face* confocal images stepping through the retinal layers of threshold injury have similar expression and characteristics to supra-threshold injury (Figure 23). Within the IPL just posterior to the INL, cell bodies approximately 10 µm in size appear to connect to structures within the ganglion cell layer.

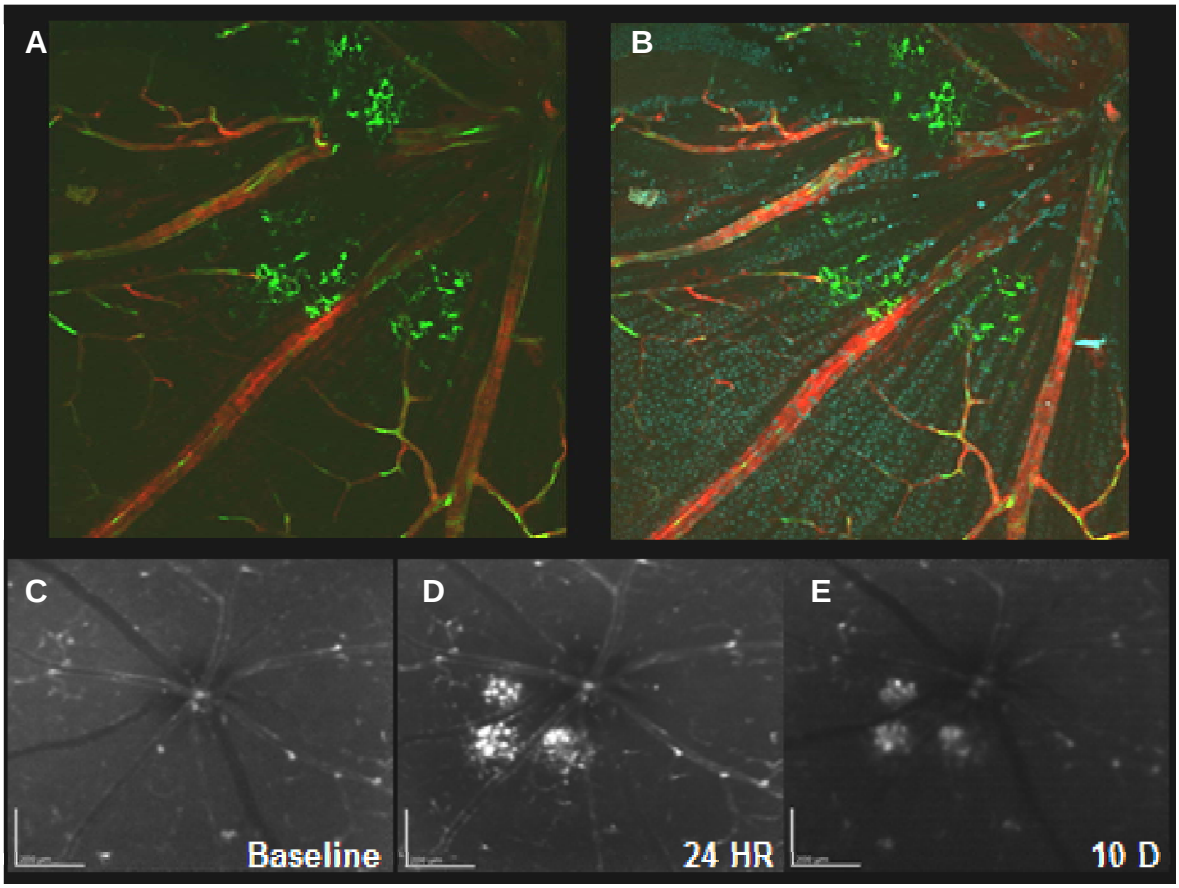

Figure 21: Fluorescence microscopy of ten day old supra-threshold retinal laser injury with complimentary *in vivo* fluorescence images from the same subject. (Top row) High quality fluorescence image of lesions (A) without DAPI and (B) with DAPI staining. (Bottom row) SLO fluorescence images of retinal fundus (C) before, (D) 24 hours, and (E) 10 days following retinal injury. Scale Bar: 200 µm

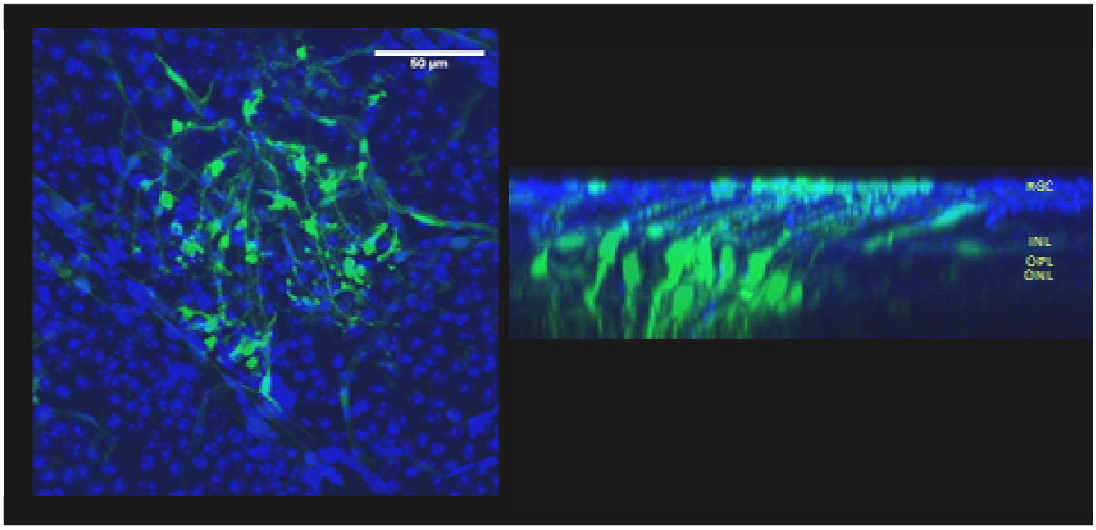

Figure 22: Fluorescence microscopy of threshold laser injury (3 day follow up) in retinal flat mount with RPE removed. (Left) Fluorescence stack image (*en face* view) focused at anterior portion of retina. EGFP expressing structures within DAPI stained retinal flat mount have a dendritic like appearance. (Right) Complimentary cross-sectional view of the same injury

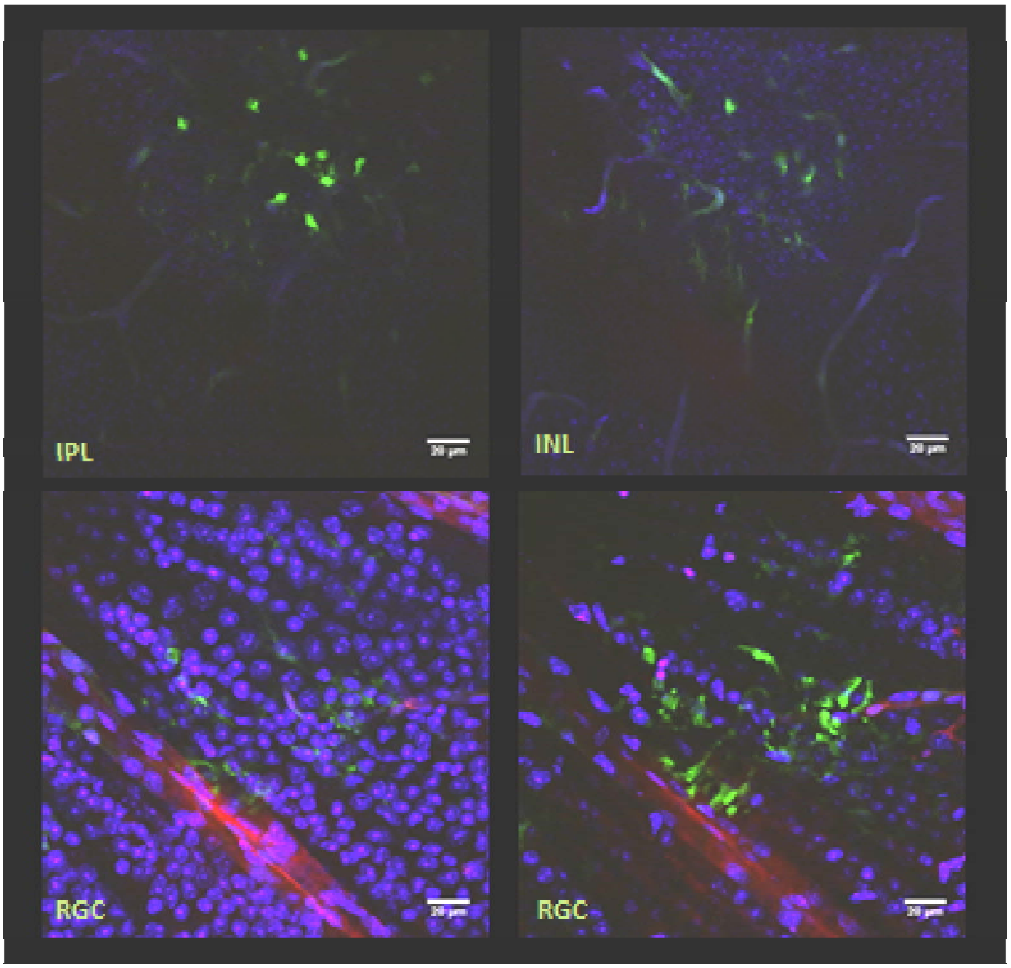

Figure 23: Fluorescence microscopy stack images (*en face* view) of threshold laser injury (3 day follow up) in retinal flat mount with RPE removed. (Top left) IPL layer with EGFP expressing cell bodies. (Top right) INL with DAPI stained cell bodies present. The cell bodies present in the IPL appear to extend into the INL. (Bottom left) RGC layer with EGFP cell bodies within the cell layers. (Bottom right) Anterior of the RGC bodies. Note EGFP cell bodies still present within this layer despite decreased number of RGC cell bodies. Scale bar: 20 µm

Localization of NF-κB (p65) activation in the mouse retina as a result of laser injury was assessed using fluorescence microscopy of retinal flat mounts and cryosections. Fluorescence microscope images collected at different depths within the neural tissue of retinal flat mounts at the lesion site confirmed the activation of NF-κB anterior to the RPE up to the inner retinal layers. Expression of NF-κB (p65) may not be specific to one neuronal cell body type following injury. Figure 24 depicts confocal stack images collected from one lesion site 3 days post laser exposure. The shape of the fluorescent EGFP expressing cell body structures differ based on localization within the retina. The cell population in Figure 24A expresses EGFP in the perinuclear region of the neuron in contrast to cell bodies in Figure 24C which have a more uniform florescent appearance. Another possibility is the EGFP expressing structures are the Müller glia which extend the full length of the retina.

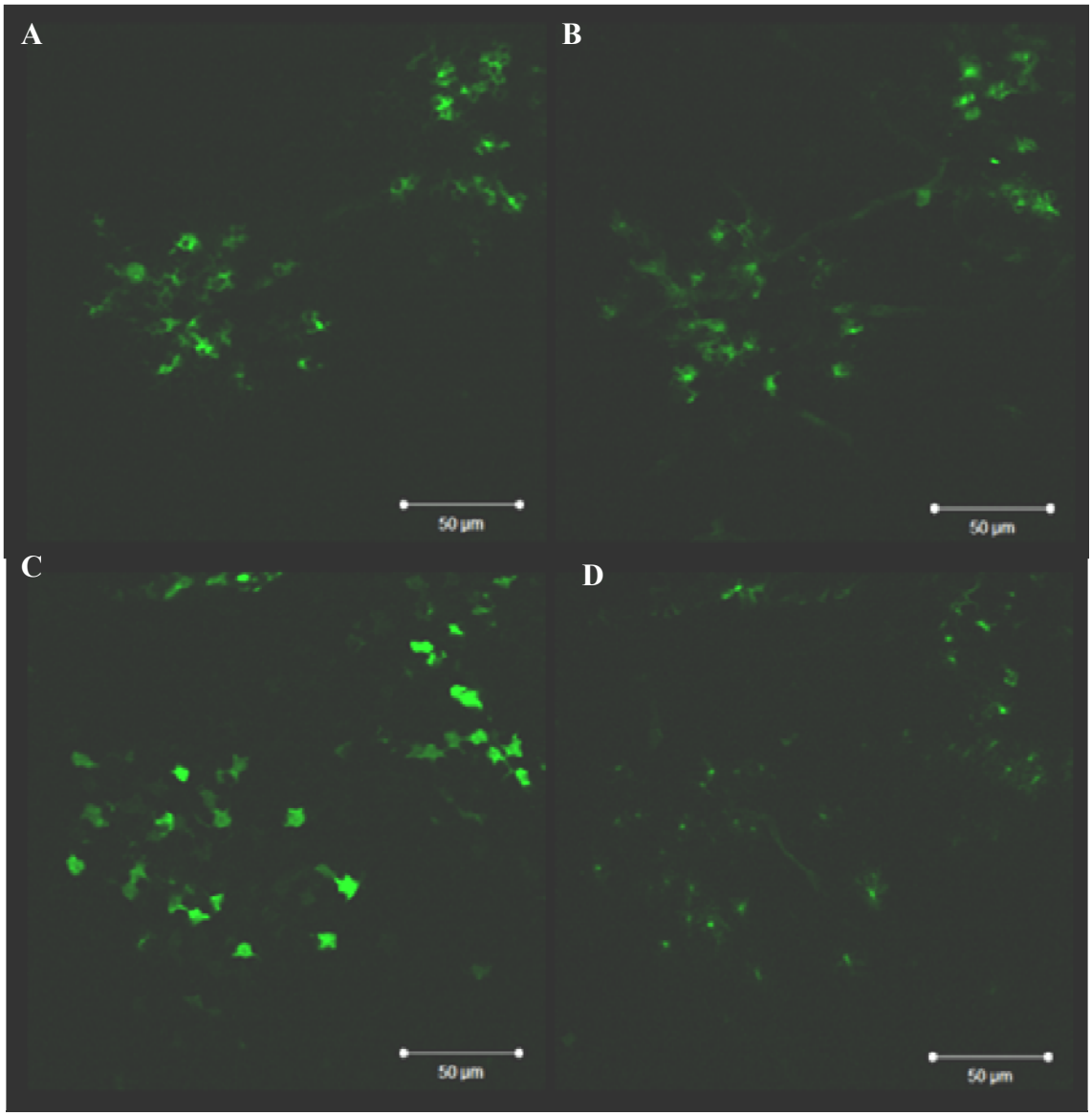

Figure 24: Fluorescence microscopy stack images (enface view) of supra-threshold laser injury (3 day follow up) in retinal flat mount with RPE removed. (A) Lesion site just above RPE (B) Retinal layer 6 µm above previous layer with the vertical ascending retinal vasculature. (C) 9 µm above the previous layer, numerous uniform fluorescent cell bodies reside and eventually connect to the dendritic cell bodies in (D). Scale bar: 50 µm

Light microscopy of retinal cryosections collected from transgenic mouse one day after receiving supra-threshold light exposures expressed EGPF in the RPE, OPL and GCL as shown in Figure 25. A TUNEL stained section of retina (Figure 26) collected from the same mouse in the previous figure reveals apoptotic cells within the ONL.

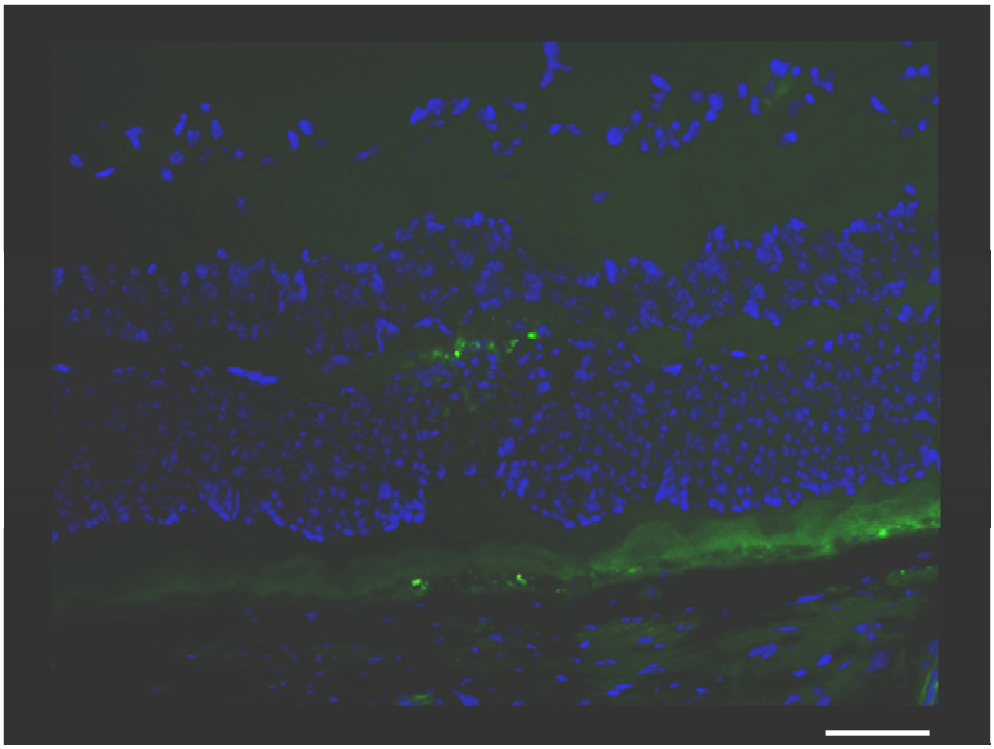

Figure 25: DAPI stained retina cross-section of a threshold laser exposure in the cis-NF-κB-EGPF mouse. Increased EGFP expression can be seen in the RPE and ONL. Scale bar: 100 µm

To determine which cell types exhibited NF-κB activation following laser injury, immunohistochemistry of retinal flatmounts and cryosections were stained using antibodies for retinal cell type markers. Müller cells span the full thickness of the retina and undergo reactive gliosis following neuronal injury. To determine if activated Müller glia participates in an NF-κB mediated inflammatory response, control and injured flatmounts were stained with anti-GFAP and anti-GS antibodies tagged with red fluorescent protein (RFP). GFAP and GS stained retina did not co-localize with EGFP indicative of NF-κB (p65) transcription in injured or control retina (Figure 27-29).

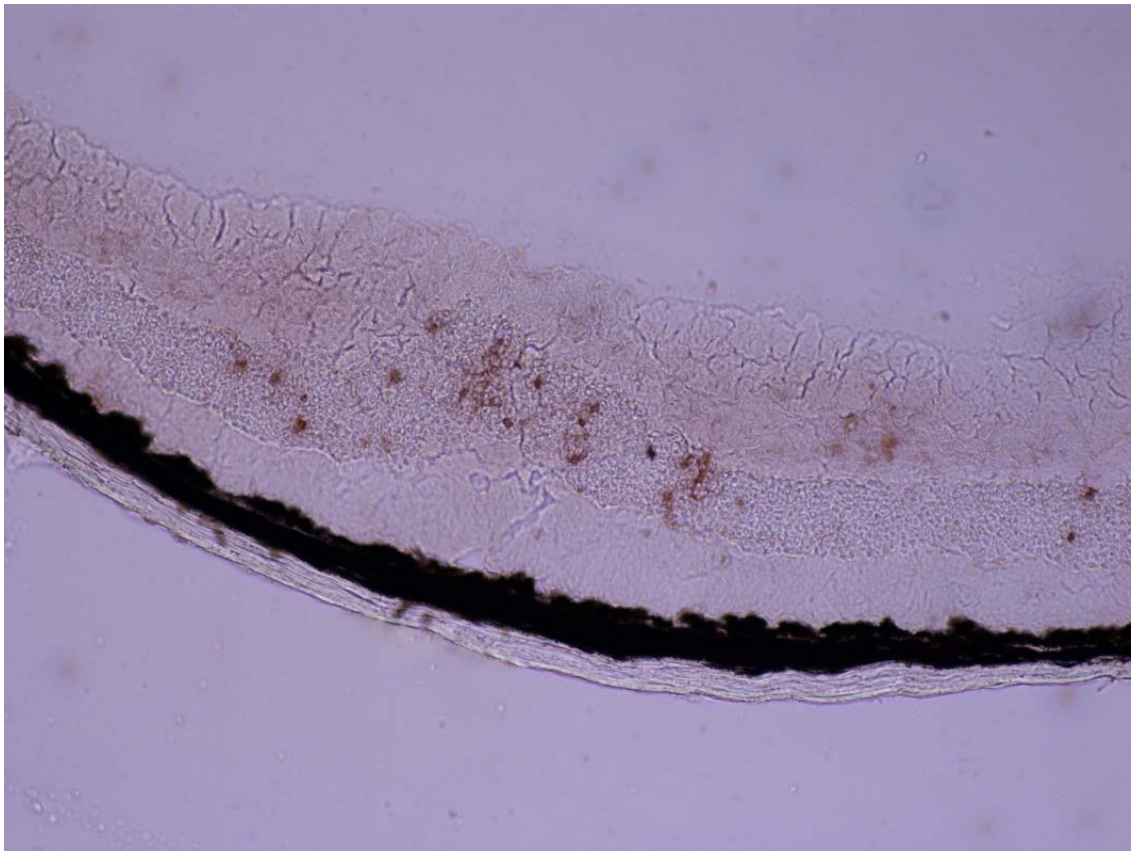

Figure 26: TUNEL stained retina cross-section of a supra-threshold laser exposure 7 days after exposure in the cis-NF-κB-EGPF mouse. Apoptotic cells are located mostly in the photoreceptor ONL

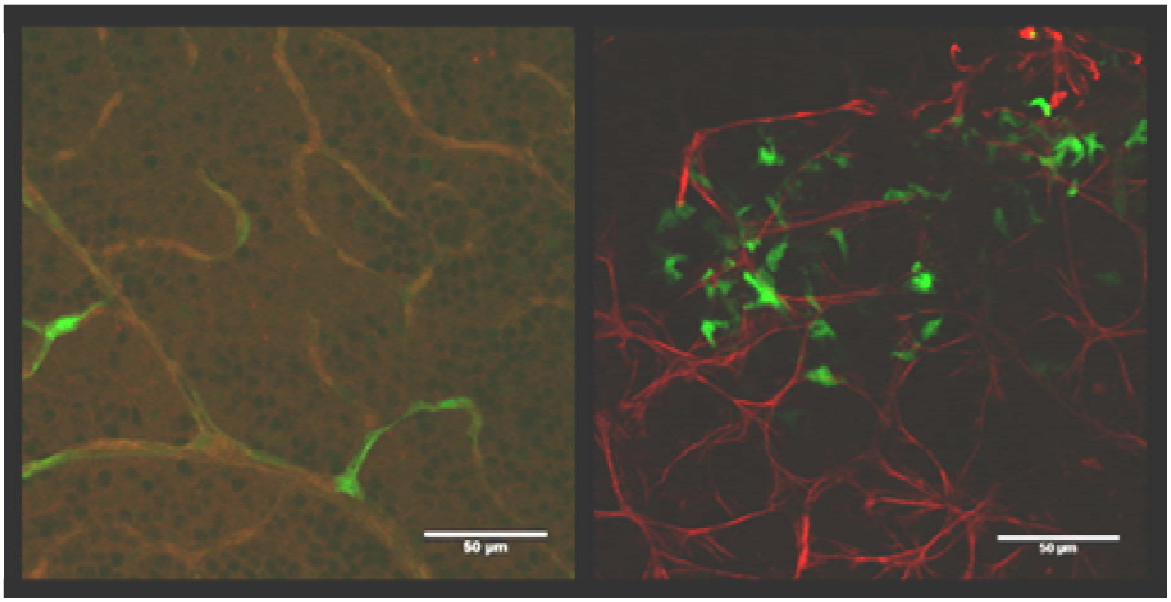

Figure 27: Fluorescence microscopy stack images (*en face* view) of non-injured retina stained with GFAP. (Left) Notice there is not any glial activation prior to injury. (Right) GFAP (red) did not co-localize with the NF-κB cell bodies (green) in a laser injured retina. Scale bar: 50 µm

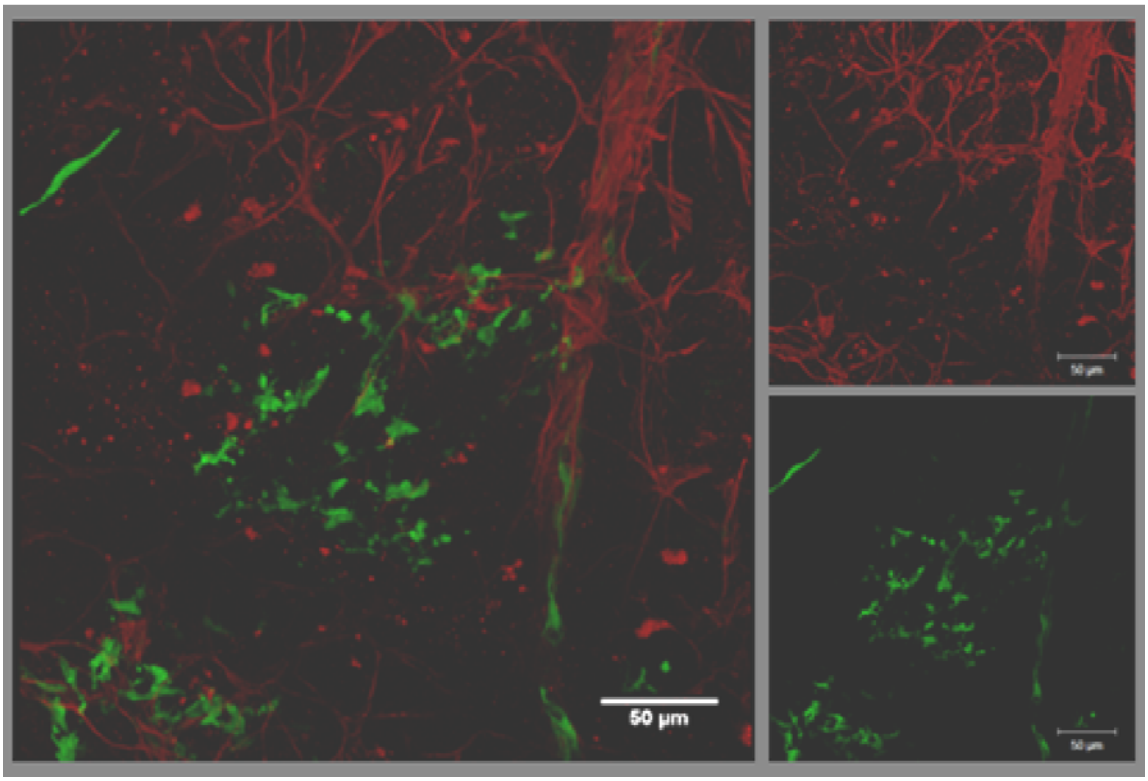

Figure 28: Another example of a fluorescence microscopy stack images (*en face* view) of injured retina stained with GFAP. (Right) GFAP (red) did not co-localize with the NF-κB cell bodies (green) in a laser injured retina. Scale bar: 50 µm

To examine the immune response of microglia and leukocyte infiltration, retinal flatmounts were stained using antibodies for IBA-1 and CD45, respectively. Neither IBA-1 nor CD45 co-localized with NF-κB in any of the retinal flatmounts imaged 3 days post exposure (Figures 30-31).

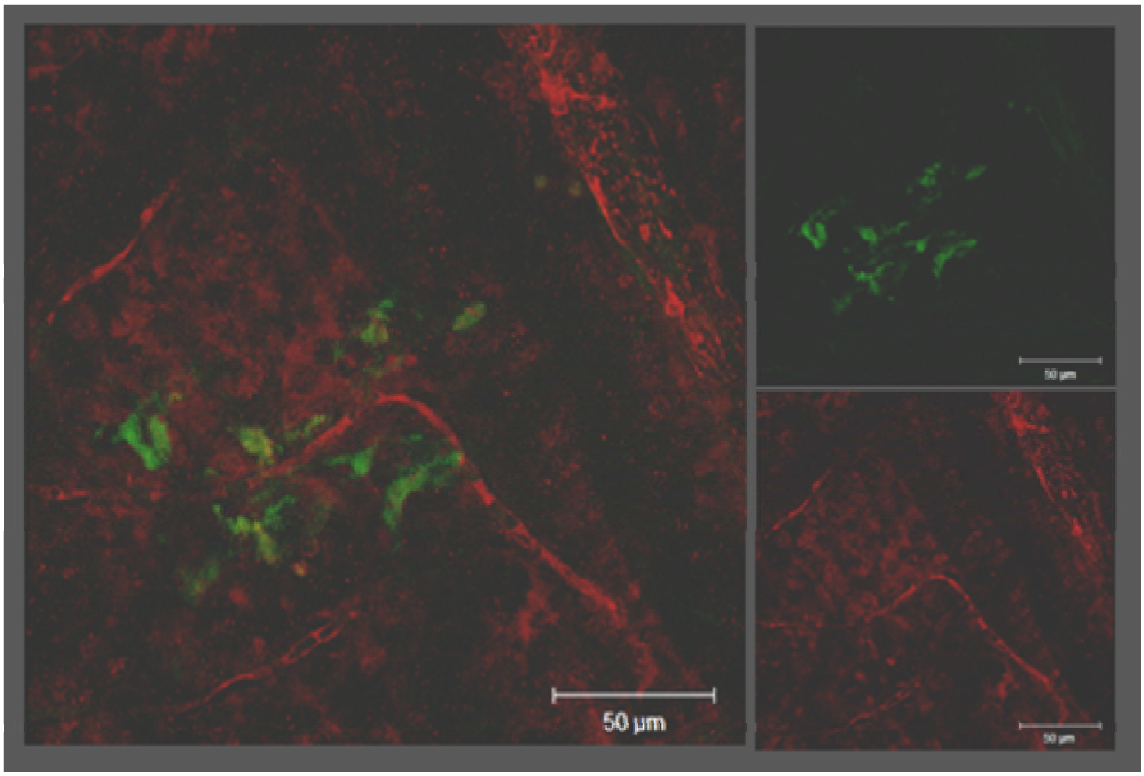

Figure 29: Fluorescence microscopy stack images (*en face* view) of injured retina stained with GS. (Right) GS (red) did not co-localize with the NF-κB cell bodies (green) in a laser injured retina. Scale bar: 50 µm

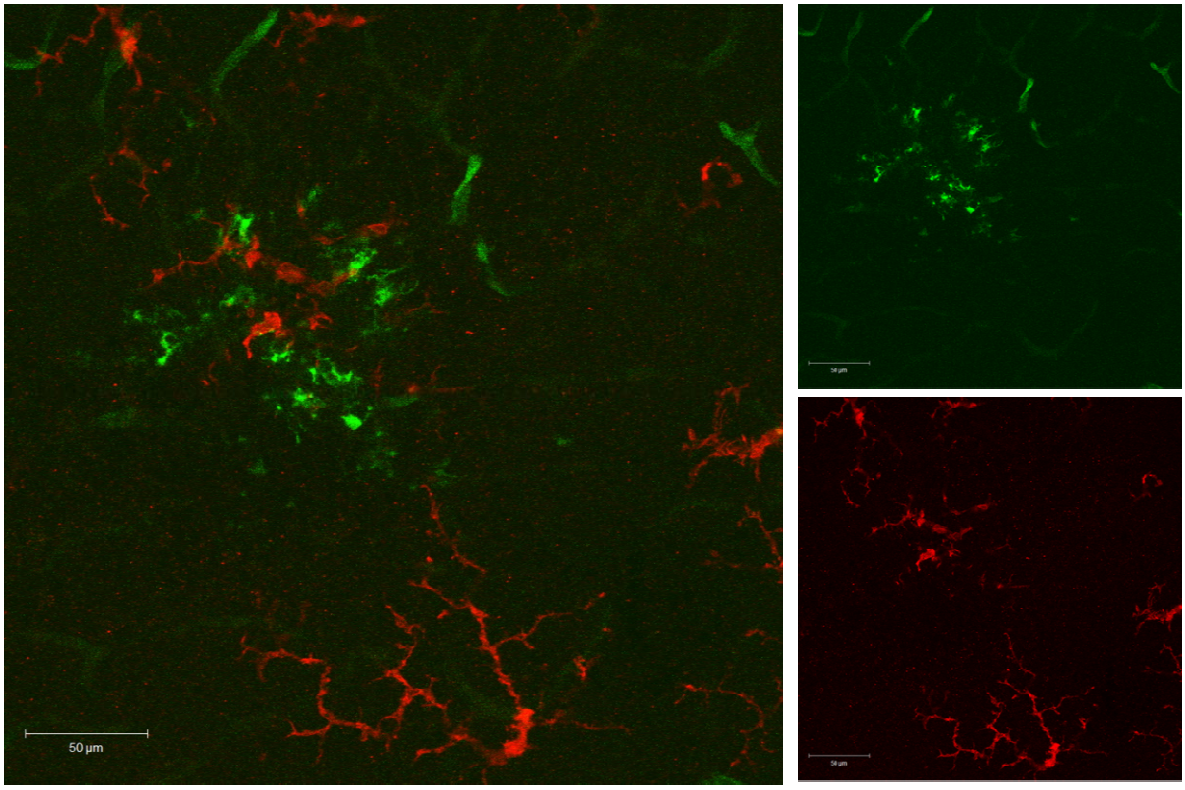

Figure 30: Fluorescence microscopy stack images (*en face* view) of injured retina stained with IBA-1. (Right) IBA-1 (red) did not co-localize with the NF-κB cell bodies (green) in a laser injured retina. Scale bar: 50 µm

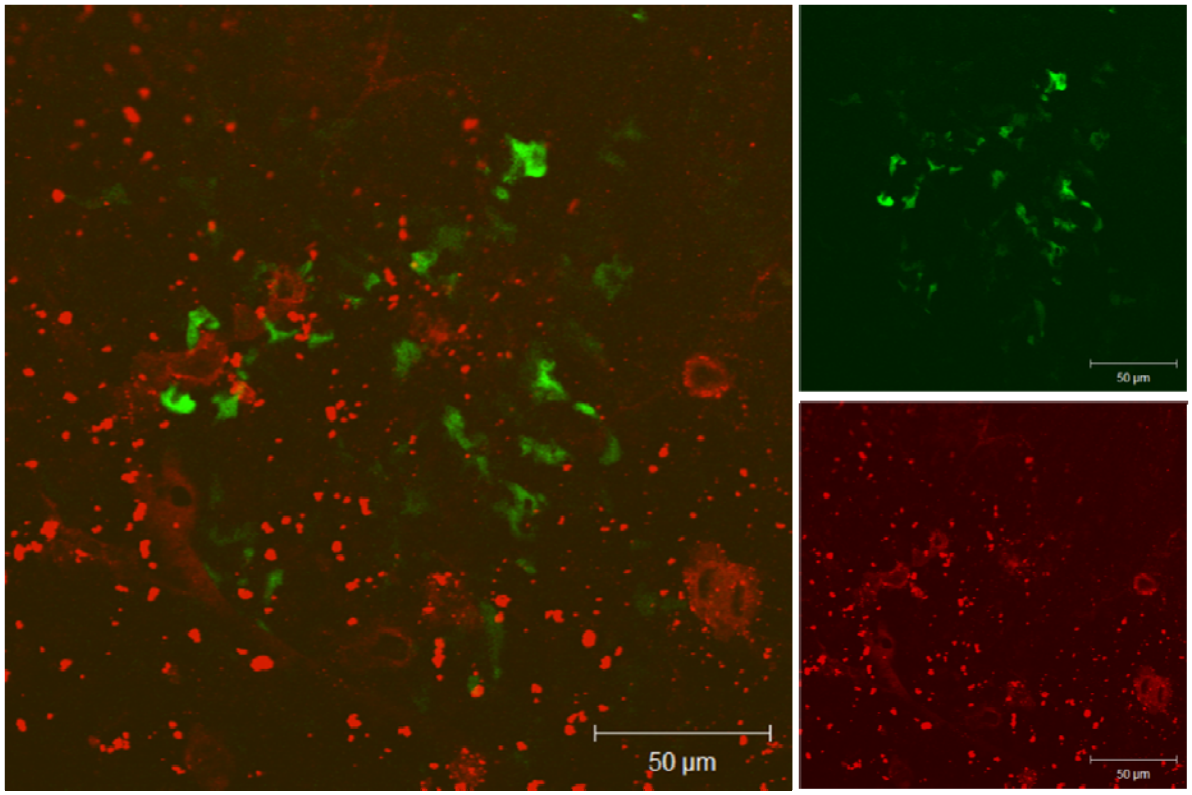

Figure 31: Fluorescence microscopy stack images (*en face* view) of injured retina stained with CD65. (Right) CD65 (red) did not co-localize with the NF-κB cell bodies (green) in a laser injured retina. Scale bar: 50 µm

4 Discussion

Fluorescence SLO imaging was used to monitor the spatial and temporal patterns of NF-κB (p65) upregulation following varying grades of laser induced damage in an EGFP reporter mouse model *in vivo*. Sub-threshold exposures were not detected using any of the available imaging modalities. Reasons for failure to detect EGFP at sub-threshold levels could be attributed to the resolution limits of the cSLO to observe weak NF-κB activation. Another possibility is that an increase in NF-κB translocation to the nucleus does not occur with exposure to sub-threshold laser exposure parameters used in this experiment. Regions of the retina exposed to threshold and supra-threshold laser damage had increased EGFP fluorescence localized to the exposed region. There was a significant relationship between the grade of laser injury (threshold versus supra-threshold) and the fluorescence intensity indicative of NF-κB (p65) transcription resulting from injury ($P=0.006$). There was significant relationship ($P=0.03$) between the observation time of the fluorescence resulting from injury and the grade of laser damage (dose), and a weak but significant correlation ($r = 0.29$, $P=0.0017$) between supra-threshold lesion size and EGFP fluorescence indicative of NF-κB transcription. In summary, the exposure irradiance dictated the level of fluorescence (indicative of NF-κB transcription) detected and as well as the duration of expression.

Immunohistochemistry and light microscopy was used to identify the retinal cell localization of NF-κB in control and laser injured mice. TUNEL assay was used to determine if NF-κB activation was associated with apoptosis. In the control retina, NF-κB (p65) positive cells were identified in the inner and outer plexiform and ganglion cell layers. The same result was found in

healthy retinal tissue of the C3H mouse.[50] Past studies of NF-κB involvement of photoreceptor degeneration and injury following intense light and thermal injury have had conflicting results.[51] NF-κB (p65) was constituently active in dark adapted photoreceptor cells of the BALB/cJ mice and in cultured mouse 661W photoreceptor cells.[22, 52] The 661 W photoreceptor cells exposed to visible light (4.5 mW/cm^2) caused oxidative damage in cells resulting in cell death accompanied by a decrease in NF-κB (p50 and p65). Wu et al. (2002) was the first to demonstrate NF-κB (p65) upregulation in photoreceptor cells after intense light exposure *in vivo* using histological methods in a BALB/cJ mouse model and was associated with apoptosis.[22] Our results are similar to Wu in that the ONL of a supra-threshold exposed transgenic mice tested positive for apoptotic cells. Thermal laser injury in rabbit retina induced NF-κB activation in the nuclei of photoreceptor cells as early as 3 hours post exposure.[53] Glickman et al. (2007) used a snake model and human RPE cells to study NF-κB activation following thermal and photo-oxidative stress induced by (0.5 W/cm^2), respectively.[54, 55] His results were not able to show whether expression of NF-κB was pro- or anti-apoptotic in both studies. Based on previous studies of thermal injury and results presented here, NF-κB expression exerts pro-apoptotic activity in photoreceptor cell bodies but not in the inner retinal cell bodies.[53, 54] For the first time, results presented here show retinal thermal laser injury induces an NF-κB mediated stress response from the lesion site up to the RGC layer. TUNEL staining did not indicate death of cell bodies in the inner retinal layers, but results were examined strictly from one mouse 3 days following supra-threshold thermal injury. Further study is needed to ascertain whether the inner retinal cells expressing NF-κB results in death or recovery.

At the onset of the laser induced trauma, damaged neurons surrounding the central lesion area create further damage to neighboring neurons through "excitotoxicity". The hypothesis of "excitotoxicity" is damaged neurons release glutamate which induces expression of the N-methyl-D-aspartate (NMDA) receptor leading to a rapid influx of Ca^{2+} into the neuron cell body leading to osmotic imbalance and consequently activates apoptosis.[56] In a more recent finding by Lebrun-Julien et al. (2009), NF-κB is "strongly" activated in the retina following NMDA exposure and induces NF-κB dependent death of retinal neurons. Furthermore, the NF-κB activity occurs in the Müller glia and not the retinal neurons.[14] NF-κB initiates endogenous production of TNFα in Müller glia and activates production of neuron surface AMPA receptors increasing Ca^{2+} permeability thus initiating excitotoxicity.[57] GFAP staining of activated Müller glia is commonly used as a marker of retinal light induced damage.[58–60] Results presented here show that laser induced NF-κB expression did not colocalize with activated Müller glial tissue in retinal flatmounts of laser injury 3 days after supra-threshold exposure. Based on microscopy images, the cytoplasm of the photoreceptor cell bodies express NF-κB following injury as well as unknown cell populations in the inner retina. IBA-1 appeared in close proximity to EGFP expressing structures but did not colocalize with NF-κB. Based on this result, it does not appear Müller cells are the source of NF-κB mediated neurotoxicity. The prolonged transcription of NF-κB 25 days after laser exposures may indicate ongoing inflammation and possible disruption to the immune privilege of the eye.[61]

The dynamics of the lesion formation and inflammation response may follow the gene response model of retinal injury described by Vázquez-Chona et al. (2004).[62] An early response to retinal injury is the upregulation of transcription factors which occurs after the injury followed by a delayed response of genes related to the cell cycle and death. In the model, NF-κB p105 and p65

were included in the early stage transcription response and were overarching transcription factors activated throughout the stages of retinal injury and repair. Our results show ongoing NF-κB translocation to the nucleus for the duration of the 1 week observations. Wu et al. (2002) reported NF-κB upregulation 12 hours post "intense" light exposure. The delayed response of retinal injury begins approximately 4 hours after injury and peaks 1-3 days later and consists of gene expression related to cell cycle, cell death, survival, inflammation, neural development, and gliosis.[62] In relation to the retinal injury model, supra-threshold lesion size measured using OCT increased over the 24 hour period with a concomitant increase in fluorescence of the GFP+ cells indicative of NF-κB transcription. The increase in lesion size 24 hours after injury has been reported in the rabbit and primate.[63] In addition, autophagy activation by NF-κB is key for cell survival after heat shock. Basal expression of NF-κB p65 plays a role in protein "quality control" by helping to clear aggregated or malformed proteins induced by autophagy induction during heat shock recovery.[64] It is hypothesized NF-κB p65 controls the clearance of protein aggregates primarily by regulating HSPB8 and BAG3 (Hsp70 co-chaperone) at the transcription level.[65] The peak expression of NF-κB at 48 hour may indicate inflammation as well as protein removal.

In regards to constitutive activity of NF-κB (p65), two-photon images in one sample of uninjured retina showed expression in the cytoplasm of inner nuclear cell bodies. Our results are similar to Cooper et al. in that NF-κB (p65) does show constituent activity in the inner retinal regions of the human retina.[66] It has been shown that constitutive NF-κB (p65) expression is required for neuronal survival in other CNS systems such as the brain.[67–69] Paradoxically, inhibition of NF-κB following neuronal injury improves recovery.[70–72] NF-κB constitutive activity was present in the arterials of the mouse retina. There are no previous studies detailing the *in vivo* monitoring of NF-κB constitutive activity of the retinal vasculature. Previous studies have reported the constitute activity in bovine and human smooth muscle cells and rat carotid artery. [73–76] Monitoring the expression of NF-κB constitutive and inducible activity in relation to angiogenesis may be possible.[77] In addition, monitoring NF-κB in relation to the effects of diet on retinal vasculature could add some insight into the development of diabetic retinopathy.[78]

5 Conclusion

Overall, we have introduced the cis-NF-κB-EGFP reporter mouse for *in vivo* studies of NF-κB (p65) activation in relation to light injury and healing in the retina. The cell-specific spatial and temporal patterns of NF-κB p65 upregulation following various grades of laser induced damage was monitored using a reporter transgenic mouse model should be further studied. Future research will seek to understand the NF-κB signaling pathways by investigating upregulation of specific proteins and the variability between expression patterns of NF-κB regulated genes based on regimes of laser damage. Inhibition of these inflammatory pathways may represent a feasible treatment strategy for laser retinal injury. Characterization of NF-κB spatial and temporal activation following laser injury may provide a useful method to assess the degree and type of injury incurred in the retina as well as establishing the dosimetry of experimental treatments related to light induced healing. The role of NF-κB in retinal excitotoxicity in retinal gliosis after light induced damage cannot be elucidated in this study. The hypothesis of Müller cell mediated excitotoxicity following injury should be further studied. Future studies will include validation of the EGFP+ cell population seen in the retina *in vivo* as peripheral white blood cells would allow monitoring of the immune response of the retina to injury *in vivo*.

6 References

1. Yanoff, M., Duker, J. S. & Augsburger. *Ophthalmology*. (Mosby Elsevier, 2009). at <http://www.clinicalkey.com/dura/browse/bookChapter/3-s2.0-B9780323043328X00017>
2. Cato, A. C. B. & Wade, E. Molecular mechanisms of anti-inflammatory action of glucocorticoids. *BioEssays* **18,** 371–378 (1996).
3. Gupta, S. C., Sundaram, C., Reuter, S. & Aggarwal, B. B. Inhibiting NF-κB activation by small molecules as a therapeutic strategy. *Biochimica et Biophysica Acta (BBA) - Gene Regulatory Mechanisms* **1799,** 775–787 (2010).
4. Lam, T. T., Takahashi, K., Fu, J. & Tso, M. O. Methylprednisolone therapy in laser injury of the retina. *Graefes Arch. Clin. Exp. Ophthalmol.* **231,** 729–736 (1993).
5. Kandari, J. A., Raizada, S. & Razzak, A. A. Accidental Laser Injury to the Eye. *Ophthalmic Surg Lasers Imaging* 1–5 (2010). doi:10.3928/15428877-20100215-26
6. Jonas JB, Martus P, Degenring RF, Kreissig I & Akkoyun I. Predictive factors for visual acuity after intravitreal triamcinolone treatment for diabetic macular edema. *Arch Ophthalmol* **123,** 1338–1343 (2005).
7. Mohamed, S. *et al.* Factors associated with variability in response of diabetic macular oedema after intravitreal triamcinolone. *Clinical & Experimental Ophthalmology* **37,** 602–608 (2009).
8. Cunningham, M. A., Edelman, J. L. & Kaushal, S. Intravitreal Steroids for Macular Edema: The Past, the Present, and the Future. *Survey of Ophthalmology* **53,** 139–149 (2008).
9. Sramek, C. *et al.* Non-damaging Retinal Phototherapy: Dynamic Range of Heat Shock Protein Expression. *IOVS* **52,** 1780–1787 (2011).
10. Ozawa, Y. *et al.* Neuroprotective Effects of Lutein in the Retina. *Curr Pharm Des* **18,** 51–56 (2012).
11. Sasaki, M. *et al.* Neuroprotective Effect of an Antioxidant, Lutein, during Retinal Inflammation. *IOVS* **50,** 1433–1439 (2009).
12. Brown Jr, J. *et al.* Steroidal and Nonsteroidal Antiinflammatory Medications Can Improve Photoreceptor Survival after Laser Retinal Photocoagulation. *Ophthalmology* **114,** 1876–1883 (2007).
13. Denton, M. L. *et al.* Damage Thresholds for Exposure to NIR and Blue Lasers in an In Vitro RPE Cell System. *IOVS* **47,** 3065–3073 (2006).
14. Gerstman, B. S. & Glickman, R. D. Activated Rate Processes and a Specific Biochemical Mechanism for Explaining Delayed Laser Induced Thermal Damage to the Retina. *J. Biomed. Opt* **4,** 345–351 (1999).
15. Wu, J., Seregard, S. & Algvere, P. V. Photochemical Damage of the Retina. *Survey of Ophthalmology* **51,** 461–481 (2006).
16. Glickman, R. D. Phototoxicity to the Retina: Mechanisms of Damage. *International Journal of Toxicology* **21,** 473–490 (2002).
17. Denton, M. L. *et al.* Spatially correlated microthermography maps threshold temperature in laser-induced damage. *J Biomed Opt* **16,** 036003 (2011).
18. Schmitz-Valckenberg, S. *et al.* Real-time in vivo imaging of retinal cell apoptosis after laser exposure. *Invest. Ophthalmol. Vis. Sci.* **49,** 2773–2780 (2008).
19. Lebrun-Julien, F. *et al.* Excitotoxic Death of Retinal Neurons In Vivo Occurs via a Non-Cell-Autonomous Mechanism. *J. Neurosci.* **29,** 5536–5545 (2009).

20. Grimm, C., Wenzel, A., Hafezi, F. & Remé, C. E. Gene expression in the mouse retina: the effect of damaging light. *Mol. Vis.* **6,** 252–260 (2000).
21. Chen, L. *et al.* Light damage induced changes in mouse retinal gene expression. *Experimental Eye Research* **79,** 239–247 (2004).
22. Wu, T., Chen, Y., Chiang, S. K. S. & Tso, M. O. M. NF-κB Activation in Light-Induced Retinal Degeneration in a Mouse Model. *IOVS* **43,** 2834–2840 (2002).
23. Noell, W. K., Walker, V. S., Kang, B. S. & Berman, S. Retinal damage by light in rats. *Invest Ophthalmol* **5,** 450–473 (1966).
24. Boretsky, A., Motamedi, M., Bell, B. & Kuijk, F. van. Quantitative Evaluation of Retinal Response to Laser Photocoagulation Using Dual-Wavelength Fundus Autofluorescence Imaging in a Small Animal Model. *IOVS* (2011). doi:10.1167/iovs.10-7033
25. Sen, R. & Baltimore, D. Multiple nuclear factors interact with the immunoglobulin enhancer sequences. *Cell* **46,** 705–716 (1986).
26. Fan, C., Yang, J. & Engelhardt, J. F. Temporal pattern of NFkappaB activation influences apoptotic cell fate in a stimuli-dependent fashion. *J. Cell. Sci.* **115,** 4843–4853 (2002).
27. Viatour, P., Merville, M.-P., Bours, V. & Chariot, A. Phosphorylation of NF-kappaB and IkappaB proteins: implications in cancer and inflammation. *Trends Biochem. Sci.* **30,** 43–52 (2005).
28. Rupec, R. A. & Baeuerle, P. A. The genomic response of tumor cells to hypoxia and reoxygenation. Differential activation of transcription factors AP-1 and NF-kappa B. *Eur. J. Biochem.* **234,** 632–640 (1995).
29. Schreck, R., Rieber, P. & Baeuerle, P. A. Reactive oxygen intermediates as apparently widely used messengers in the activation of the NF-kappa B transcription factor and HIV-1. *EMBO J* **10,** 2247–2258 (1991).
30. Bachelerie, F., Alcami, J., Arenzana-Seisdedos, F. & Virelizier, J. L. HIV enhancer activity perpetuated by NF-kappa B induction on infection of monocytes. *Nature* **350,** 709–712 (1991).
31. Hang, C.-H., Shi, J.-X., Li, J.-S., Li, W.-Q. & Yin, H.-X. Up-regulation of intestinal nuclear factor kappa B and intercellular adhesion molecule-1 following traumatic brain injury in rats. *World J. Gastroenterol.* **11,** 1149–1154 (2005).
32. Haas, A. F. *et al.* Redox regulation of wound healing? NF-kappaB activation in cultured human keratinocytes upon wounding and the effect of low energy HeNe irradiation. *Free Radic. Biol. Med.* **25,** 998–1005 (1998).
33. Nomoto, Y. *et al.* Expression of nuclear factor kappaB and tumor necrosis factor alpha in the mouse brain after experimental thermal ablation injury. *Neurosurgery* **48,** 158–166 (2001).
34. Sondén, A., Johansson, A.-S. M., Palmblad, J. & Kjellström, B. T. Proinflammatory reaction and cytoskeletal alterations in endothelial cells after shock wave exposure. *J. Investig. Med.* **54,** 262–271 (2006).
35. Dvoriantchikova, G. *et al.* Inactivation of astroglial NF-κB promotes survival of retinal neurons following ischemic injury. *Eur J Neurosci* **30,** 175–185 (2009).
36. Sramek, C. *et al.* Non-damaging Retinal Phototherapy: Dynamic Range of Heat Shock Protein Expression. *IOVS* **52,** 1780–1787 (2011).
37. Albarracin, R., Eells, J. & Valter, K. Photobiomodulation Protects the Retina from Light-Induced Photoreceptor Degeneration. *IOVS* **52,** 3582–3592 (2011).

38. Yu, P. K., Cringle, S. J., McAllister, I. L. & Yu, D.-Y. Low power laser treatment of the retina ameliorates neovascularisation in a transgenic mouse model of retinal neovascularisation. *Experimental Eye Research* **89,** 791–800 (2009).
39. Gonzalez-Lima, F. & Rojas. Low-level light therapy of the eye and brain. *Eye and Brain* 49 (2011). doi:10.2147/EB.S21391
40. Eells, J. T. *et al.* Therapeutic photobiomodulation for methanol-induced retinal toxicity. *PNAS* **100,** 3439–3444 (2003).
41. Desmet, K. D. *et al.* Clinical and Experimental Applications of NIR-LED Photobiomodulation. *Photomedicine and Laser Surgery* **24,** 121–128 (2006).
42. Eells, J. T. *et al.* Mitochondrial signal transduction in accelerated wound and retinal healing by near-infrared light therapy. *Mitochondrion* **4,** 559–567 (2004).
43. Rojas, J. C., Lee, J., John, J. M. & Gonzalez-Lima, F. Neuroprotective Effects of Near-Infrared Light in an In Vivo Model of Mitochondrial Optic Neuropathy. *J. Neurosci.* **28,** 13511–13521 (2008).
44. Chen, A. C.-H. *et al.* Low-Level Laser Therapy Activates NF-kB via Generation of Reactive Oxygen Species in Mouse Embryonic Fibroblasts. *PLoS ONE* **6,** e22453 (2011).
45. Huang, Y.-Y., Sharma, S. K., Carroll, J. & Hamblin, M. R. Biphasic Dose Response in Low Level Light Therapy – An Update. *Dose Response* **9,** 602–618 (2011).
46. Chung, H. *et al.* The nuts and bolts of low-level laser (light) therapy. *Ann Biomed Eng* **40,** 516–533 (2012).
47. Alexander, G., Carlsen, H. & Blomhoff, R. Corneal NF-kappaB activity is necessary for the retention of transparency in the cornea of UV-B-exposed transgenic reporter mice. *Exp. Eye Res.* **82,** 700–709 (2006).
48. Carlsen, H., Moskaug, J. Ø., Fromm, S. H. & Blomhoff, R. In Vivo Imaging of NF-κB Activity. *J Immunol* **168,** 1441–1446 (2002).
49. Magness, S. T. *et al.* In Vivo Pattern of Lipopolysaccharide and Anti-CD3-Induced NF-κB Activation Using a Novel Gene-Targeted Enhanced GFP Reporter Gene Mouse. *J Immunol* **173,** 1561–1570 (2004).
50. Zeng, H., Tso, M. O. M., Lai, S. & Lai, H. Activation of nuclear factor-κB during retinal degeneration in rd Mice. (2008). at <http://www.molvis.org/molvis/v14/a128/>
51. Crawford, M. J. *et al.* Bcl-2 Overexpression Protects Photooxidative Stress-Induced Apoptosis of Photoreceptor Cells via NF-κB Preservation. *Biochemical and Biophysical Research Communications* **281,** 1304–1312 (2001).
52. Krishnamoorthy, R. R. *et al.* Photo-oxidative stress down-modulates the activity of nuclear factor-kappaB via involvement of caspase-1, leading to apoptosis of photoreceptor cells. *J. Biol. Chem.* **274,** 3734–3743 (1999).
53. Wang, H.-C. H. NF-B Activation in Laser-Induced Retinal Injury in Rabbits. in **D837,** (2008).
54. Glickman, R. D., Elliott III, W. R. & Kumar, N. Functional and cellular responses to laser injury in the rat snake retina. in **6435,** 643511–643511–11 (2007).
55. Glickman, R. D. *et al.* Intracellular signaling mechanisms responsive to laser-induced photochemical and thermal stress. 260–269 (2005). doi:10.1117/12.584135
56. Parsons, C. G., Danysz, W. & Quack, G. Glutamate in CNS disorders as a target for drug development: an update. *Drug News Perspect.* **11,** 523–569 (1998).
57. Lebrun-Julien, F. *et al.* Excitotoxic death of retinal neurons in vivo occurs via a non-cell-autonomous mechanism. *J. Neurosci.* **29,** 5536–5545 (2009).

58. Albarracin, R., Eells, J. & Valter, K. Photobiomodulation Protects the Retina from Light-Induced Photoreceptor Degeneration. *IOVS* **52,** 3582–3592 (2011).
59. De Raad, S., Szczesny, P. J., Munz, K. & Remé, C. E. Light damage in the rat retina: glial fibrillary acidic protein accumulates in Müller cells in correlation with photoreceptor damage. *Ophthalmic Res.* **28,** 99–107 (1996).
60. Izumi-Nagai, K. *et al.* Macular Pigment Lutein Is Antiinflammatory in Preventing Choroidal Neovascularization. *Arterioscler Thromb Vasc Biol* **27,** 2555–2562 (2007).
61. Qiao, H., Lucas, K. & Stein-Streilein, J. Retinal Laser Burn Disrupts Immune Privilege in the Eye. *Am J Pathol* **174,** 414–422 (2009).
62. Vázquez-Chona, F., Song, B. K. & Geisert, E. E. Temporal Changes in Gene Expression after Injury in the Rat Retina. *IOVS* **45,** 2737–2746 (2004).
63. Leibu, R. *et al.* Development of laser-induced retinal damage in the rabbit. *Graefe's Archive for Clinical and Experimental Ophthalmology* **237,** 991–1000 (1999).
64. Nivon, M., Richet, E., Codogno, P., Arrigo, A.-P. & Kretz-Remy, C. Autophagy activation by NFkappaB is essential for cell survival after heat shock. *Autophagy* **5,** 766–783 (2009).
65. Nivon, M. *et al.* NF-kappa B regulates protein quality control after heat stress through modulation of the BAG3-HspB8 complex. *J. Cell Sci.* **125,** 1141–1151 (2012).
66. Fan, W. & Cooper, N. G. F. Glutamate-induced NFkappaB activation in the retina. *Invest. Ophthalmol. Vis. Sci.* **50,** 917–925 (2009).
67. Bhakar, A. L. *et al.* Constitutive nuclear factor-kappa B activity is required for central neuron survival. *J. Neurosci.* **22,** 8466–8475 (2002).
68. Fridmacher, V. *et al.* Forebrain-Specific Neuronal Inhibition of Nuclear Factor-κB Activity Leads to Loss of Neuroprotection. *J. Neurosci.* **23,** 9403–9408 (2003).
69. Piccioli, P. *et al.* Inhibition of nuclear factor-κB activation induces apoptosis in cerebellar granule cells. *Journal of Neuroscience Research* **66,** 1064–1073 (2001).
70. Fu, E. S. *et al.* Transgenic inhibition of glial NF-kappa B reduces pain behavior and inflammation after peripheral nerve injury. *Pain* **148,** 509–518 (2010).
71. Brambilla, R. *et al.* Inhibition of astroglial nuclear factor κB reduces inflammation and improves functional recovery after spinal cord injury. *J Exp Med* **202,** 145–156 (2005).
72. Brambilla, R. *et al.* Transgenic inhibition of astroglial NF-κB leads to increased axonal sparing and sprouting following spinal cord injury. *Journal of Neurochemistry* **110,** 765–778 (2009).
73. Lawrence, R., Chang, L. J., Siebenlist, U., Bressler, P. & Sonenshein, G. E. Vascular smooth muscle cells express a constitutive NF-kappa B-like activity. *J. Biol. Chem.* **269,** 28913–28918 (1994).
74. Bellas, R. E., Lee, J. S. & Sonenshein, G. E. Expression of a constitutive NF-kappa B-like activity is essential for proliferation of cultured bovine vascular smooth muscle cells. *J Clin Invest* **96,** 2521–2527 (1995).
75. Jung, Y. D. *et al.* Role of P38 MAPK, AP-1, and NF-kappaB in interleukin-1beta-induced IL-8 expression in human vascular smooth muscle cells. *Cytokine* **18,** 206–213 (2002).
76. Lindner, V. The NF-kappaB and IkappaB system in injured arteries. *Pathobiology* **66,** 311–320 (1998).
77. Stahl, A. *et al.* The Mouse Retina as an Angiogenesis Model. *IOVS* **51,** 2813–2826 (2010).
78. Kowluru, R. A. & Chan, P.-S. Oxidative Stress and Diabetic Retinopathy. *Exp Diabetes Res* **2007,** (2007).